TÉCNICO LISBOA

B Physics Anomalies from Dark Matter

Tomás Costa Lopes

Thesis to obtain the Master of Science Degree in

Engineering Physics

Supervisors: Prof. Rui Alberto Serra Ribeiro dos Santos
Prof. João Paulo Ferreira da Silva

Examination Committee

Chairperson:	Prof. Mário João Martins Pimenta
Supervisor:	Prof. Rui Alberto Serra Ribeiro dos Santos
Members of the Committee:	Prof. Jorge Manuel Rodrigues Crispim Romão

October 2022

Dedicated to Arca

Acknowledgments

First of all, I am grateful to my supervisors, Prof. Rui Santos and Prof. João Paulo Silva for all their support, patience and knowledge provided. I extend my gratitude to Rodrigo, for all the help in this project, and to the remaining Prof. Rui's students for many useful Physics discussions. I could not finish this paragraph without mentioning my other particle's friend Sérgio, who always helped me whenever I needed and kept me company through all these fun quantum field courses.

I would also like to thank all the friends that have been with me in this five-year journey: to Miguel, Maria and Bernardo, who despite all the online bullying were still funny at times, to Filipa for her kindness, compassion and always checking on me (like a mother would), to my nemesis Zeca, to Zé, to Santos and of course to Manel, my best friend whom I carried on every single project we did together (I would not have it any other way). I also want to mention my juvenile friends Félix, Rafa and Luís, who were a joy to be around in all these years. Last, but definitely not least, I thank my guardian angels, Ivo and Piçarra, who always pushed me in the right direction. In this course, you helped me endlessly and always inspired me through your knowledge and work, even on this very paragraph.

Finally, I would like to show some appreciation to my hometown support, which was essential to my success and well-being during my time at Técnico. To my friends Mamede, Serra, Mariano and Alexandre, thank you for all the happy moments. To my family, I am grateful for their unconditional love and support throughout these years, with a special mention to my mother's potato soup which always gave me comfort.

I am grateful to CFTP for the financial support given through the BL44-2022 fellowship. This work has been partially supported by *Fundação para a Ciência e Tecnologia* (FCT), under the project CFTP UIDP/00777/2020 - IST-ID.

Resumo

Neste trabalho estudamos uma extensão do Modelo Padrão ao comparar dois modelos que explicam a origem de indícios de violação de universalidade de sabor dos leptões para o decaimento $b \to s l^+ l^-$, o momento anómalo do muão $(g-2)$ e o problema da matéria escura (ME). O decaimento do quark b e a anomalía do muão $(g-2)$ são explicados através de diagramas com *loops* onde participam os candidatos a ME. Para além dos campos do Modelo Padrão, os modelos têm um campo fermiónico sem cor, um campo escalar sem cor e um com cor. Num dos modelos, o fermião é um dubleto de $SU(2)_L$ e os escalares são singletos de $SU(2)_L$ enquanto no outro modelo o fermião é um singleto de $SU(2)_L$ e os escalares são dubletos de $SU(2)_L$. Após estudarmos a fenomenologia de sabor e matéria escura dos modelos, fazemos um *scan* de forma a encontrar o espaço de parâmetros dos modelos que explica os três fenómenos de nova física simultaneamente. Concluímos que ambos os modelos conseguem explicar não só todos os problemas mencionados anteriormente mas também outros problemas de sabor e ME. Contudo, existem diferenças cruciais na forma como as restrições na ME afetam os dois modelos, resultando numa diferença considerável nos valores permitidos para a massa de ME.

Palavras-chave: modelo de nova física; decaimento do *quark* b; matéria escura; momento anómalo do muão;

Abstract

In this work we study an extension of the Standard Model by comparing two models which explain the origin of the experimental hints of lepton flavor universality violation in $b \to s l^+ l^-$ decays, the long-standing muon $(g-2)$ anomaly and the dark matter (DM) problem. The b decays and the muon $(g-2)$ anomalies are explained by additional one-loop diagrams with DM candidates. Besides the Standard Model fields, the models have a colourless fermion field, a colourless scalar field and a coloured scalar field. In one model the fermion is an $SU(2)_L$ doublet and the scalars are $SU(2)_L$ singlets, while in the other the fermion is an $SU(2)_L$ singlet and the scalars are $SU(2)_L$ doublets. After studying the dark matter and flavour physics phenomenology of the models, we perform a parameter scan and search for the parameter space of the models which explains all three new physics phenomena simultaneously. We conclude that both models can explain all previously mentioned issues simultaneously while also satisfying other flavour and DM constraints. However, there are crucial differences between how the DM constraints affect the two models, leading to a noticeable difference in the allowed DM mass.

Keywords: new physics model, b quark decay, dark matter, anomalous moment of the muon;

Contents

List of Tables

List of Figures

Chapter 1

Background Concepts

1.1 Standard Model

The Standard Model of particle physics (SM) is currently the most accepted theory used to describe the strong, weak and electromagnetic interactions between elementary particles. It started being developed in the 1960s [1] and throughout the years has shown to be extremely successful in providing useful predictions for experimental results, with the last big discovery being the Higgs particle in 2012 [2].

The SM is a gauge theory, meaning it is built by imposing a set of local continuous symmetries on the fields. In this case, it obeys the gauge symmetry $SU(3)_c \times SU(2)_L \times U(1)_Y$, where c, L and Y represent the color, left-handed component of the field and the hypercharge, given by $Y = Q - T_3$ where Q is the electric charge of the particle and T_3 is the third component of the isospin. One can separate the fermionic fields in left and right-handed components:

$$\psi = \psi_L + \psi_R, \quad \psi_L = \frac{1-\gamma_5}{2}\psi, \quad \psi_R = \frac{1+\gamma_5}{2}\psi\,. \tag{1.1}$$

The symmetry $SU(2)_L$ is implemented such that the left and right-handed fields live in two different representations: left-handed fields are organized in an $SU(2)_L$ doublet while right-handed fields lie in an $SU(2)_L$ singlet. The fields which compose the SM are organized in three families of leptons, three families of quarks and one Higgs family:

$$\begin{aligned}
&Q_L = \begin{pmatrix} U_L \\ D_L \end{pmatrix} = \left\{ \begin{pmatrix} u_L \\ d_L \end{pmatrix}, \begin{pmatrix} c_L \\ s_L \end{pmatrix}, \begin{pmatrix} t_L \\ b_L \end{pmatrix} \right\}_{Y=+1/6}, \; U_R = \{u_R, c_R, t_R\}_{Y=+2/3}, \; D_R = \{d_R, s_R, b_R\}_{Y=-1/3}, \\
&L_L = \left\{ \begin{pmatrix} \nu_{e_L} \\ e_L \end{pmatrix}, \begin{pmatrix} \nu_{\mu_L} \\ \mu_L \end{pmatrix}, \begin{pmatrix} \nu_{\tau_L} \\ \tau_L \end{pmatrix} \right\}_{Y=-1/2}, L_R = \{e_R, \mu_R, \tau_R\}_{Y=0}, \\
&\Phi = \begin{pmatrix} \phi^+ \\ \phi^0 \end{pmatrix}.
\end{aligned} \tag{1.2}$$

In order to verify gauge invariance, it is necessary to introduce new gauge vector fields

$$SU(3)_c \to G_a^\mu,\ a=(1,...,8) \qquad SU(2)_L \to W_b^\mu,\ b=(1,2,3) \qquad U(1)_Y \to B^\mu \tag{1.3}$$

and promote the derivatives of fields to the correspondent covariant derivatives. For the colourless doublet fermion and the Higgs doublet, the derivative is as follows

$$\partial_\mu \psi_L \to D_\mu \psi_L = \left(\partial_\mu - ig'Y B_\mu - i\frac{g\tau_i W_\mu^i}{2}\right)\psi_L\,, \tag{1.4}$$

while for the coloured doublet fermion we get

$$\partial_\mu q_L \to D_\mu q_L = \left(\partial_\mu - ig'Y B_\mu - i\frac{g\tau_i W_\mu^i}{2} - i\frac{g_s G_\mu^a \lambda^a}{2}\right) q_L\,, \tag{1.5}$$

where $\tau_i, i=(1,2,3)$ are the Pauli matrices and $\lambda_a, a=(1,...,8)$ are the Gell-mann matrices. For the colourless and coloured singlets, we obtain respectively:

$$\partial_\mu l_R \to D_\mu l_R = (\partial_\mu - ig'Y B_\mu)\, l_R \qquad \partial_\mu u_R \to D_\mu u_R = \left(\partial_\mu - ig'Y B_\mu - i\frac{g_s G_\mu^a \lambda^a}{2}\right) u_R\,. \tag{1.6}$$

The full SM Lagrangean is given by

$$\mathcal{L}_{SM} = \mathcal{L}_{gauge} + \mathcal{L}_f + \mathcal{L}_H + \mathcal{L}_Y\,. \tag{1.7}$$

The first term corresponds to the gauge sector

$$\mathcal{L}_{gauge} = -\frac{1}{4}\left(B_{\mu\nu}B^{\mu\nu} + W_{\mu\nu}^a W^{\mu\nu a} + G_{\mu\nu}^a G^{\mu\nu a}\right)\,, \tag{1.8}$$

with

$$B_{\mu\nu} = \partial_\mu B_\nu - \partial_\nu B_\mu\,, \quad W_{\mu\nu}^a = \partial_\mu W_\nu^a - \partial_\nu W_\mu^a + g\epsilon^{abc} W_\mu^b W_\nu^c\,, \quad G_{\mu\nu}^a = \partial_\mu G_\nu^a - \partial_\nu G_\mu^a + g_s f^{abc} G_\mu^b G_\nu^c\,, \tag{1.9}$$

where ϵ^{abc} and f^{abc} are the structure constants for the $SU(2)$ and $SU(3)$ groups, respectively [3]. The second term describes the fermionic terms

$$\mathcal{L}_f = -i\bar{Q}_L\gamma^\mu D_\mu Q_L - i\bar{U}_R\gamma^\mu D_\mu U_R - i\bar{D}_R\gamma^\mu D_\mu D_R - i\bar{L}_L\gamma^\mu D_\mu L_L - i\bar{C}_R\gamma^\mu D_\mu L_R\,, \tag{1.10}$$

where $\bar{\psi} = \psi^\dagger\gamma^0$ and $\mu=(0,1,2,3)$. The third term corresponds to the scalar potential

$$\mathcal{L}_H = (D^\mu\phi)^\dagger D_\mu\phi - \mu^2|\phi|^2 - \lambda|\phi|^4\,, \tag{1.11}$$

where ϕ is the Higgs scalar field and μ^2, λ are real parameters. From this potential, the Higgs field

undergoes a spontaneous symmetry breaking (SSB)

$$SU(3)_c \times SU(2)_L \times U(1)_Y \rightarrow SU(3)_c \times U(1)_{EM}\,. \tag{1.12}$$

For $\mu^2 < 0$ and $\lambda > 0$, the Higgs field is able to acquire a non-zero vacuum expectation value (vev) that changes the minimum in the potential v

$$\left.\frac{\partial \mathcal{L}_{Higgs}}{\partial |\phi|^2}\right|_{\varphi=0} = 0 \Leftrightarrow \mu^2 + \lambda v^2 = 0 \rightarrow v = \sqrt{\frac{-\mu^2}{\lambda}}\,, \tag{1.13}$$

where $v \approx 246 GeV$ and $\langle \phi^\dagger \phi \rangle_0 = v/2$. We can now expand the scalar fields around its minimum.

$$\phi = \langle \phi \rangle_0 + \varphi = \frac{1}{\sqrt{2}} \begin{pmatrix} 0 \\ v \end{pmatrix} + \begin{pmatrix} G^+ \\ \frac{1}{\sqrt{2}}(G^0 + h) \end{pmatrix}\,. \tag{1.14}$$

According to the Goldstone theorem, a massless scalar arises for each generator of a continuous global symmetry that is not a symmetry of the vacuum. Therefore, the theory gains three massless bosons $G^\pm$, G^0. These three bosons are then absorbed in the Higgs mechanism [4] as the longitudinal components of the Z, $W^\pm$ bosons for them to become massive. Moreover, we obtain a massive scalar, the Higgs boson with mass $m_H = -2\mu^2$. Finally, the fourth term is responsible for generating the masses of the SM fermions

$$\mathcal{L}_Y = -\bar{Q_L}\tilde{\phi} Y^u U_R - \bar{Q_L}\phi Y^d D_R - \bar{L_L}\phi Y^l L_R + h.c.\,, \tag{1.15}$$

where $\tilde{\phi} = i\tau_2 \phi^*$ and Y^μ, Y^d, Y^l are 3×3 complex matrices in flavour space. After SSB, we perform a basis change on the fermionic fields

$$\bar{l_L} = U_{L_L}\bar{L_L} \qquad \bar{l_R} = U_{L_R}\bar{L_R} \qquad \bar{u_L} = U_{u_L}\bar{U_L} \qquad \bar{d_L} = U_{D_L}\bar{D_L} \qquad \bar{u_R} = U_{U_R}\bar{U_R} \qquad \bar{d_R} = U_{D_R}\bar{D_R}\,, \tag{1.16}$$

where $\bar{l_L}$, $\bar{l_R}$, $\bar{u_L}$, $\bar{d_L}$, $\bar{u_R}$, $\bar{d_R}$ define the mass eigenbasis. The mass eigenstates of the fermions are therefore given by

$$\begin{aligned} M_U &= diag(m_u, m_c, m_t) = \frac{v}{\sqrt{2}} U^\dagger_{L_L} Y^u U_{U_R}\,, \\ M_D &= diag(m_d, m_s, m_b) = \frac{v}{\sqrt{2}} U^\dagger_{D_L} Y^d U_{D_R}\,, \\ M_L &= diag(m_e, m_\mu, m_\tau) = \frac{v}{\sqrt{2}} U^\dagger_{L_L} Y^l U_{L_R}\,, \end{aligned} \tag{1.17}$$

and finally one can use the matrices U_{U_L} and U_{D_L} to write the Cabibbo-Kobayashi-Maskawa matrix (CKM) as

$$V_{CKM} = U^\dagger_{U_L} U_{D_L} = \begin{pmatrix} V_{ud} & V_{us} & V_{ub} \\ V_{cd} & V_{cs} & V_{cb} \\ V_{td} & V_{ts} & V_{tb} \end{pmatrix}\,, \tag{1.18}$$

which contains all information regarding the strength of the flavour-changing weak interaction. In 2020,

the absolute values of these parameters were given by [5]

$$\begin{pmatrix} |V_{ud}| & |V_{us}| & |V_{ub}| \\ |V_{cd}| & |V_{cs}| & |V_{cb}| \\ |V_{td}| & |V_{ts}| & |V_{tb}| \end{pmatrix} = \begin{pmatrix} 0.97370 \pm 0.00014 & 0.2245 \pm 0.0008 & 0.00382 \pm 0.00024 \\ 0.221 \pm 0.004 & 0.987 \pm 0.011 & 0.0410 \pm 0.0014 \\ 0.0080 \pm 0.0003 & 0.0388 \pm 0.0011 & 1.013 \pm 0.030 \end{pmatrix}. \quad (1.19)$$

1.2 Dark Matter

1.2.1 Historical context

One of the biggest mysteries in physics over the last century is Dark Matter: the universe behaves in a way that the visible matter we are able to observe is only a small fraction of the total matter present in the universe. There is a fraction of the matter in the universe that does not emit light and which interactions are unknown. It is therefore referred to as Dark Matter. Despite many efforts from the scientific community to discover its properties, no model to describe it has ever been proven to be correct and its nature remains a mystery.

The first time DM was detected was in 1933 [6], where the values for the velocities of the galaxies in the Coma cluster were observed to be much larger than the ones that would be associated to the known matter: these would be fast enough to escape the gravitational pull of the cluster and set free from the orbit. In 1936, the same behaviour was observed on the Virgo cluster by Smith. In 1939, Babcock used an optical spectroscopy method to obtain the velocity of rotation of the Andromeda galaxy and found that, far away from the center, its value was also much higher than what was expected from the mass of the visible galaxy. In the 1970s, the concept of dark matter became widely accepted. Stronger evidences of its existence came from the rotation of the Andromeda (1970) and other large galaxies (1974), indicating a pattern. However, this behaviour did not change the spatial distribution of the structures. In 1973, Ostriker & Peebles [7] showed that galactic disks on their own would not be stable structures and suggested that these would have to be surrounded by dark spherical halos, a property common to all galaxies.

1.2.2 The nature of dark matter

From the beginning, many DM candidates were taken into consideration. First, it was believed that its nature would be baryonic (three-quark particles), with DM structures being ionized gases (1972), low mass stars (1975) and collapsed objects (1975). However, through the study of cosmic microwave background radiation (CMBR), the baryon density in the universe can be obtained and has a value of $\Omega_{bar} \approx 0.045$ which is a small fraction of the dark matter abundance $\Omega_{DM} \approx 0.3$ and thus its nature cannot be just baryonic: non-baryonic dark matter must also exist.

Cowsik & McClelland [8] suggested in 1973 the first non baryonic candidate for the role of DM, the neutrino. Since most matter in the universe is dark, it would be expected for DM to influence greatly the formation of large structures like galaxies and galaxy clusters. However if the DM particles were to be relativistic (called hot dark matter), like a neutrino, it would be a very hard challenge to explain the

formation of these structures: at the time of matter-radiation equality in the early universe, the formation of low scale structures would not be possible. Instead, galaxy-cluster concentrations of structures would collapse first while smaller structures such as individual galaxies would form subsequently. However, observations of galaxies at high redshift allow us to discard this scenario and conclude that smaller scale structures were formed first and the larger structures were formed later. The formation of structures can however be explained by non-baryonic non-relativistic matter, with particle velocity $v \ll c$, called Cold Dark Matter(CDM). This was first considered by Primack (1982) [9], Peebles (1982) [10] and Blumenthal (1984) [11] and to this day, it is still believed that the CDM models are the most likely to be correct.

Another strong evidence of the existence of DM comes from Cosmic Microwave Background (CMB) observation, which suggest that the energy density in the universe has a value of

$$\rho_0 \approx \frac{3H_0^2}{8\pi G_N} \approx 10^{-29} g \cdot cm^{-3}\,, \tag{1.20}$$

where $H_0 \approx 70$ km s^{-1} Mpc^{-1} is the Hubble constant and $G_N = 6.67 \times 10^{-11}$ N m kg^{-2} is the Newton gravitational constant. This energy density value can only be explained through the existance of DM, with a contribution of 70% dark energy, 26% dark matter and 4% luminous (or ordinary) matter. From CMB data, by observing the distribution of galaxies on large scales (LSS) and by studying the contribution of ordinary ordinary matter and DM, through Big Bang Nucleosynthesis (BBN), one can obtain the amount of DM in the universe

$$\Omega_{DM} = \frac{\rho_{DM,0}}{\rho_0} \approx 0.26\,, \tag{1.21}$$

where the 0 subscript represents the density value evaluated today.

The most popular mechanism considered to explain the amount of DM present in the universe is called the Freeze-Out mechanism: In the early universe, DM was assumed to be in thermal equilibrium with the remaining matter (with the DM conversion to ordinary being at an equal rate as the SM matter conversion into DM). However, as the universe expanded and its temperature decreased, the cross section of the process of DM annihilation to ordinary matter decreased and therefore the thermal equilibrium could no longer be maintained, leading the DM relic density to stabilize at the value in equation 1.21.

1.2.3 Known properties

Nowadays, there are some already known properties of a DM particle [12]: its lifetime must be longer than the current age of the universe, it also does not interact electromagnetically in order to not emit photons (otherwise it would have already been detected) and therefore it must be neutral. Moreover, for DM collisional effects to be considered, the mean free path of a DM particle λ_{DM} must be larger than a typical size of a cluster of galaxies ≈ 1 Mpc, which has a density of $\rho_{cl} \approx 1$ GeV cm^{-3}. Therefore, one must verify

$$\lambda_{DM} = \frac{1}{\sigma \rho_{cl}/m} > 1 \rightarrow \sigma/m \approx 1 barn/GeV\,, \tag{1.22}$$

which is of the order of a strong interaction. This suggests that the DM may not be colisionless and self interactions may be allowed. Also, it can interact with other SM particles as long as no photons

are emitted in the process. Good DM candidates are massive particles that only interact via weak interactions and gravitational force, called WIMPS. Its abundance must also verify the currently observed DM density in the universe $\Omega_{DM} \approx 0.26$, which is achieved by some WIMP models. Many experiments have been developed in order to probe DM particle models, with the more advanced searches being on WIMP models. Some experiments include searches for signals from elastic scattering of DM particles off nucleons (direct detection), DM annihilation or decay processes (indirect detection) and production of DM particles at colliders with additional detectable SM particles. WIMP models are the most popular family among the theories used to explain DM. In these models, the DM candidate cannot interact using the strong or electromagnetic force, otherwise it would be visible. Moreover, the mass range is of the order $\mathcal{O}(GeV) - \mathcal{O}(TeV)$ and therefore can be classified as CDM. Another widely considered family of models are the Massive Astrophysical Compact Halo Objects (MACHOs), which consist of large astrophysical objects which do not emit much light and whose non-baryonic constituent particles are heavier than WIMPs. These structures can be detected through a method called gravitational lensing: when a halo passes in front of a background star, its gravitational field distorts the light emitted from the star and amplifies its brightness, allowing us to detect the halo. However, studies that used this technique [13] found a large number of MACHOs with masses around 0.5 times the Sun's mass in the Milky way and concluded that these structures only provide an explanation to 20% of the DM mass, with the missing portion still remaining a mystery.

The current abundance of the DM particle remaining from the beginning of the universe, that is, the Big Bang is called the DM relic density. To compute this quantity, we assume that the relic density is determined by a freeze-out mechanism: in the early universe, due to very high temperatures, the cross section of the creation and annihilation DM process was a lot larger and therefore DM and SM particles were in thermal equilibrium, with production and annihilation of DM happening at an equal rate and the DM density being at a higher value. However, as the universe expanded and grew colder, the cross section of the DM production process decreased and consequently the abundance of DM in the universe also decreased, stabilizing in the fixed value we know today, given by [14]:

$$\Omega_{DM} = 0.1199 \pm 0.0022\,. \tag{1.23}$$

1.2.4 DM direct detection

DM direct detection (DD) experiments are the ones attempting to detect DM particle signals directly by observing its interactions with ordinary matter. It is certainly known from cosmology and astrophysical observations mentioned before that DM interacts through the gravitational force with ordinary matter. Regarding other forces, the scientific community is still unsure of DM interacts with baryonic matter and therefore a large number of theoretical possibilities are available. The DM DD experiments must take into account how much DM is present in the experimental apparatus, how it will interact with ordinary matter (and of course how we can distinguish the DM signals from other interactions between ordinary matter) and how can we detect it in the laboratory.

Over the last few decades, many experiments were developed with the goal of observing these DM

signals. In this work we will focus on WIMP DD experiments, where the considered process is the scattering of DM with ordinary matter, where the latter may be in the form of a nucleon. At first sight,

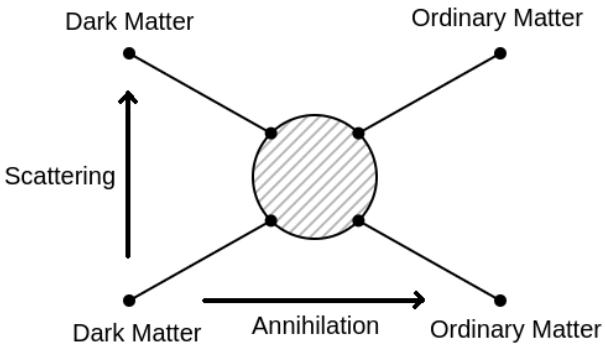

Figure 1.1: Diagram of DM scattering with ordinary matter and annihilation to ordinary matter.

this would look like a fairly simple experiment to assemble. However, the challenge here is that the properties of DM particles are unknown and thus it is hard to constrain the parameter space of the DM model (with the most relevant being its mass) and predict the interaction signals to be observed. Let us consider a DD WIMP scattering experiment: The DM distribution in our galaxy can be described in a structure called a DM Halo [15], which consists on a spherical region containing gravitationally bounded matter. The DM obeys a Maxwell-Boltzmann distribution [16]

$$f(v) = \frac{1}{\sqrt{2\pi}\sigma} \exp\left\{-\frac{|v^2|}{2\sigma^2}\right\}, \tag{1.24}$$

where v is the velocity of the WIMP particles and σ is the velocity dispersion. We can roughly define the local velocity v_c as the velocity of our galaxy and the dispersion given by

$$\sigma = \sqrt{\frac{3}{2}} v_c \,, \tag{1.25}$$

with $v_c = 2.2 \times 10^5$ m s^{-1}. If we are considering a scattering experiment, we are assuming that besides the gravitational interactions, DM also interacts with ordinary matter through other types of forces such as weak interactions. Considering the collision between the DM particle and a heavy nucleon at rest, if we consider a WIMP χ with a mass of $100GeV$, its kinetic energy is given by $K = \frac{1}{2} m_\chi v_c^2 \approx 27$ keV . Since a heavy nucleon binding energy is of the order $6 - 8$ keV, there is not enough energy for nucleon fission to happen and we may assume that the collision is elastic. As a consequence, the WIMP will transfer some energy to the nucleon and it is our goal to observe it (and distinguish it from eventual collisions between the nucleon and other SM particles). Following [16], the maximum transfered energy from the collision from a WIMP with velocity v is given by the expression

$$E_R^{max} = 2\frac{\mu^2 v^2}{m_N} \,, \tag{1.26}$$

where m_N is the nucleon mass and

$$\mu = \frac{m_N m_\chi}{m_N + m_\chi}\,, \tag{1.27}$$

is the reduced mass of the system. Now if we consider an experiment where the target of the WIMPs is the nucleon of an atom, the differential event rate is given by [11]

$$\frac{dR}{dE_R} = \frac{R_0}{E_0 r}\exp\left\{-\frac{E_R}{E_0 r}\right\}, \tag{1.28}$$

where R is the rate of the scattering events, E_R is the energy transfered to the nucleon, E_0 is the most probable recoil energy (according to the Maxwell-Boltzmann distribution) and $r = \frac{4 m_\chi m_N}{(m_\chi + m_N)^2}$. R_0 is the total event rate, given by the expression

$$\int_0^{+\infty} \frac{dR}{dE_R} = R_0\,, \tag{1.29}$$

and finally, the mean recoil energy is

$$\langle E_R \rangle = E_0 r = \left(\frac{1}{2} m_\chi v_c^2\right) r\,. \tag{1.30}$$

The detection of this energy recoil in the nucleons is the basis of the DD experiments. However, while attempting to observe this interaction, we must take into account unwanted nuclear and electric interactions from other SM particles which may contaminate our data.

1.3 B Physics

A B meson is a particle which is composed of a bottom anti-quark $\bar{b}$ and either an up quark u (B^+), a down quark d (B^0), a strange quark s (B_s^0) or a charm quark c (B_c^+). The B meson is able to decay via weak interactions to other particles. The quarks that undergo the weak interaction are not the strong interaction mass eigenstates, but linear combinations of these states. A basis can be chosen such that the up-quark (u, c and t) weak and mass eigenstates coincide, while for the down-quark (d, s and b) states obey the following relation

$$\begin{pmatrix} d' \\ s' \\ b' \end{pmatrix} = V_{CKM} \begin{pmatrix} d \\ s \\ b \end{pmatrix}\,, \tag{1.31}$$

where d, s and b are the mass eigenstates, d', s' and b' are the weakly interacting eigenstates and V_{CKM} is the CKM matrix 1.18:

The more relevant B meson processes are the following [17]: Diagrams a), b) correspond to the decays with the largest decay rate. Moreover, the decay b) is also important since it allows us to measure the CKM couplings V_{cb} and V_{ub}. Decay f) is a loop diagram which is responsible for rare decays where NP signals may reside, as we will discuss ahead.

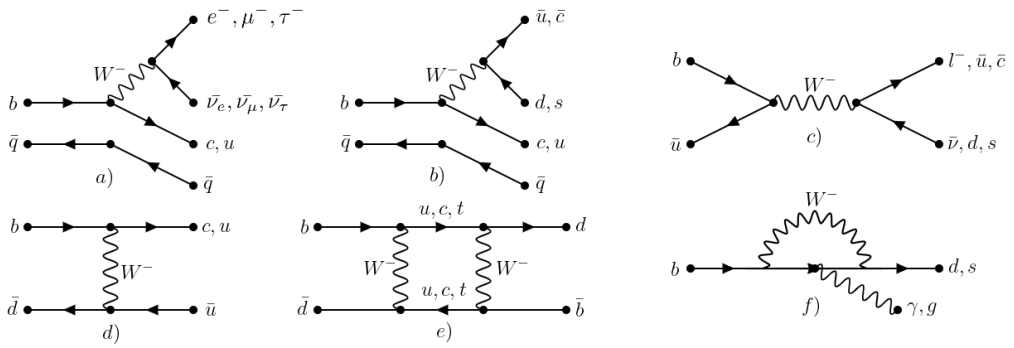

Figure 1.2: B meson possible decays.

1.4 Anomalous magnetic dipole moment

1.4.1 Magnetic moment

Before explaining our current NP problem, we first need to cover a basic concept in Physics: the magnetic moment, which is a vector quantity $\boldsymbol{m}$ consisting of the magnetic strength and direction of an object when subjected to a magnetic field. The torque $\boldsymbol{\tau}$ acting on an object due to the external magnetic field magnetic $\boldsymbol{B}$ can be written as:

$$\boldsymbol{\tau} = \boldsymbol{m} \times \boldsymbol{B} \,. \tag{1.32}$$

The magnetic moment $\boldsymbol{m}$ is closely related to the angular momentum of a particle $\boldsymbol{L}$ through what is called the gyromagnetic effect. The ratio between the magnetic moment and angular momentum is given by the value γ, called the gyromagnetic ratio:

$$\boldsymbol{m} = \gamma \boldsymbol{L} \,. \tag{1.33}$$

Let us look at the example of a single particle spinning around some axis: the angular momentum is given by

$$\boldsymbol{L} = \boldsymbol{r} \times \boldsymbol{p} = \mu \boldsymbol{r} \times \boldsymbol{v} \,, \tag{1.34}$$

where μ is the mass of the particle, $\boldsymbol{r}$ is its distance to the axis and $\boldsymbol{v}$ is its velocity. We also define the magnetic moment as

$$\boldsymbol{m} = \frac{1}{2} e \boldsymbol{r} \times \boldsymbol{v} \,, \tag{1.35}$$

where q is the electric charge of the particle. Comparing both expressions, one concludes that the value of γ is

$$\gamma = \frac{q}{2\mu} \,. \tag{1.36}$$

When we consider quantum effects, we must also take into account the intrinsic angular momentum of a particle: its spin. If the particle is an electron, the gyromagnetic constant now has the value

$$\gamma_e = \frac{-e}{2m_e} g_e \,, \tag{1.37}$$

where e is the absolute value of the electron electric charge, m_e is the electron mass and g_e is a quantity called the g-factor which must describe the intrinsic magnetic moment of the particle and the configuration.

1.4.2 Anomalous magnetic moment

For the electron, one can use the Dirac equation to predict that this quantity has an absolute value of 2. However, this value is different from the result obtained experimentally

$$|g_e| = 2.0023193043625635 \pm 0.000000000000017\,. \tag{1.38}$$

The reason is that above leading order, more complex processes such as virtual lines and loop diagrams add an "anomalous" contribution to the particle magnetic moment. The difference between these two quantities is the anomalous magnetic moment denoted by a:

$$a = \frac{g-2}{2}\,. \tag{1.39}$$

For the electron, the calculation of the anomalous moment in lowest order gives us a value of [3]

$$a_e^1 = \frac{\alpha}{2\pi} \approx 0.0011614 \tag{1.40}$$

and currently this value has been calculated up until fifth order $\mathcal{O}(\alpha^5)$:

$$a_e^5 = 0.001159652181643(764)\,. \tag{1.41}$$

This result agrees with the experimental result [18] up to the tenth figure:

$$a_e^{exp} = 0.00115965218073(28)\,. \tag{1.42}$$

For the muon, the scenario is more complicated, since we must consider contributions from more processes. The Standard Model prediction for the anomalous moment of the muon is given by

$$a_\mu^{SM} = a_\mu^{QED} + a_\mu^{EW} + a_\mu^{Hadron} = 0.00116591804(51)\,, \tag{1.43}$$

where a_μ^{QED} refers to loop contributions from photons and leptons, a_μ^{EW} takes into account the Z, W and H bosons and a_μ^{Hadron} represents the hadron loops. However the experimental value obtained at BNL is

$$a_\mu^{exp} = 0.0011659209(6)\,, \tag{1.44}$$

which represents a significative difference. In April 2021 FermiLab published a new result for the anomalous magnetic moment of $a_\mu^{exp} = 0.00116592040(54)$ which deviates 4.2σ from the Standard model prediction [19].

1.5 Effective field theories

Some very useful methods used in Physics, and more specifically in particle flavour physics to describe weak processes are Effective field theories (EFT). These techniques consist on approximations that focus on the specific degrees of freedom needed to explain a physical phenomenon at a given scale (it could be a distance or energy value per example) while neglecting others degrees of freedom at different scales. In particle physics, while studying a process, it is common to use an energy scale in order to sort out the different regimes where we can apply these theories: if we are performing an experiment at an energy scale E, we do not need to know exactly what happens at a scale $\Lambda \gg E$. Instead, we can simply characterize the theory using a set of effective parameters needed to explain the physical observables, which values can be obtained experimentally [20], together with a set of operators built by using objects of the original theory.

When considering extensions of the SM, it is possible to account for new particles and their interactions using an EFT method, with the most popular one being the SMEFT. This model obeys the same local gauge symmetry $SU(3)_c \times SU(2)_L \times U(1)_Y$ and its Lagrangean is built like the SM's, with its terms formed by gauge invariant products of the fields. However, while the SM Lagrangean terms are up to dimension 4, in the SMEFT one can consider terms with larger dimensions and the Lagrangean can be written in terms of an expansion of the SM Lagrangean 1.7

$$\mathcal{L}_{SMEFT} = \mathcal{L}_{SM} + \frac{1}{\Lambda}\sum_i c_i^{(5)}\mathcal{O}_i^{(d=5)} + \frac{1}{\Lambda^2}\sum_i c_i^{(6)}\mathcal{O}_i^{(d=6)} + \frac{1}{\Lambda^3}\sum_i c_i^{(7)}\mathcal{O}_i^{(d=7)} + \dots, \tag{1.45}$$

where $\mathcal{O}_i^D$ are the additional gauge invariant operators of dimension D, built from objects of the original theory, and c^i are parameters obtained experimentally that must account for the physical observables, called Wilson coefficients. Finally, Λ is the suppressing energy scale we consider: by taking a sufficiently large Λ (or working with a sufficiently low energy in the experiment), one can neglect the higher dimension contributions and only consider the operators necessary to describe the interactions we need. In this way one can think of the SM as a low energy limit of the more complete theory SMEFT.

Chapter 2

Introduction

Although the SM is currently the best theory to describe particle physics, it still leaves some aspects of the universe to be explained (such as neutrino masses, baryon asymmetry in the universe, among other problems), leading us to believe that the theory is in fact incomplete and needs to incorporate new physics to account for all these observations. A recent hint of NP is the observed anomaly in the semileptonic decay rate of the B meson, which suggests a violation of lepton flavour universality: The measurement of the ratios of the branching fractions

$$R(K^{(*)}) = \frac{\mathcal{B}(B \to K^{(*)}\mu^+\mu^-)}{\mathcal{B}(B \to K^{(*)}e^+e^-)} \tag{2.1}$$

was obtained by the LHCb Collaboration [21–23] with values

$$R(K) = 0.846^{+0.060+0.016}_{-0.054-0.014}, \quad q^2 \in [1,1,6]GeV^2 \tag{2.2}$$

and

$$R(K^{(*)}) = \begin{cases} 0.660^{+0.110}_{-0.070} \pm 0.024, & q^2 \in [0.045, 1.1]GeV^2 \\ 0.685^{+0.113}_{-0.069} \pm 0.047 & q^2 \in [1.1, 6]GeV^2 \end{cases}, \tag{2.3}$$

where q^2 is the dilepton mass squared in the process. However, the Standard model predictions [24, 25] are

$$R(K) = 1.0004(8), \quad q^2 \in [1,1,6]GeV^2 \tag{2.4}$$

and:

$$R(K^{(*)}) = \begin{cases} 0.920 \pm 0.007, & q^2 \in [0.045, 1.1]GeV^2 \\ 0.996 \pm 0.002 & q^2 \in [1.1, 6]GeV^2 \end{cases}. \tag{2.5}$$

Moreover, the Belle collaboration also measured these quantities with larger error bars than the LHCb results [26, 27]. One should note that these experimental results are clean probes of NP: the discrepancies in the values $R(K^{(*)})$ cannot be due to unconsidered QCD effects since the hadronic terms in the expression cancel out [24]. Additionally, the measurements of other observables in B meson decays also support the existence of anomalies. These include differential branching ratios [28–30] and angular

distributions in the decays $B \to \phi\mu^+\mu^-$ and $B \to K^{(*)}\mu^+\mu^-$ [31–38] which also deviate from the SM predictions. All of these observables are ultimately related to the $b \to s\mu^+\mu^-$ transition. Many proposals have been introduced in order to solve these discrepancies, with the most popular solutions being to introduce a boson Z' [39–43], a leptoquark [44–50] (see [51] for a review) or new exotic particles which generate one-loop penguin and box diagrams [52–56].

There are also other important hints of new physics like the long-standing low energy flavour anomaly involving the measurement of the anomalous magnetic moment of the muon $(g-2)_\mu$ [57, 58]. The most recent prediction of this quantity in the SM [59] has a 4.2σ discrepancy from the experimental measurement [60, 61]. If we define Δa_μ as the experimental difference between the experimental measurement value a_μ^{exp} and the SM prediction a_μ^{SM}, we obtain

$$\Delta a_\mu = a_\mu^{\text{exp}} - a_\mu^{SM} \approx (251 \pm 59) \times 10^{-11}\,, \tag{2.6}$$

where the error results from a combination of the theoretical and experimental uncertainties. It is expected in the future that results from J-PARC [62] and Fermilab [63] will be able to reduce this experimental uncertainty.

The goal of this work is to solve the problems mentioned above while simultaneously providing an origin for a DM candidate. The DM problem has already been investigated in models [64] which also address the B meson decay anomalies such as [65–79] for Z' models, [80–87] for leptoquark models, and [88–93] for models with one-loop solutions. In a previous work [14] a model was proposed by extending the work [91] which added three new fields to the SM: an $SU(3)_c$ coloured scalar which is also an $SU(2)_L$ singlet, Φ_3, one $SU(2)_L$ singlet colourless scalar, Φ_2, and one $SU(2)_L$ doublet vectorlike fermion, χ, with $0, \pm 1$ electric charge. In this work we will discuss a new model where instead the scalars are $SU(2)_L$ doublets and the fermion is an $SU(2)_L$ singlet. We wish to understand what is the role played by the group representations in providing a simultaneous solution to the three problems. While the Yukawa Lagrangian has a similar structure, the scalar potential is different in the two cases. More importantly, in this new model the scalars will couple to gauge bosons giving rise to the possibility of a change in DM related observables.

Chapter 3

The Model

In the previous work [14], a model was considered where three new fields were added to the SM:

- A colourless scalar ϕ_2;
- A coloured scalar ϕ_3;
- A vectorlike fermion χ which may have a charge 0 or ± 1.

In that work (model 5), the scalars were $SU(2)_L$ singlets while the fermion was an $SU(2)_L$ doublet. Our goal is to compare it to the scenario where scalars are $SU(2)_L$ doublets and the fermion is an $SU(2)_L$ singlet: this model will be called model 3. The complete set of quantum numbers is shown in Table 3.1 for models 3 and 5.

	$SU(3)_c$	$SU(2)_L$	$U(1)_Y$
χ_R	1	1	-1
ϕ_2	1	2	$1/2$
ϕ_3	3	2	$7/6$

	$SU(3)_c$	$SU(2)_L$	$U(1)_Y$
χ	1	2	$-1/2$
ϕ_2	1	1	0
ϕ_3	3	1	$2/3$

Table 3.1: Charge assignment of the new fields for model 3 (left) and model 5 (right).

where all fields are odd under a Z_2 symmetry, meaning that the allowed terms in the potential are formed by field combinations where each field may only appear an even number of times (and the allowed terms have at most mass dimension 4). The Yukawa Lagrangean 3.1 connects the dark sector with the SM one and is necessary to explain the B anomalies via one-loop diagrams. The charge of the new particles is defined by the interaction

$$\mathcal{L}_{int}^{NP} = y_{Qi}\bar{Q}_{Li}\phi_3\chi_R + y_{Li}\bar{L}_{Li}\phi_2\chi + h.c.\,, \tag{3.1}$$

where y_{Qi} and y_{Li} are constants, Q_{Li} and L_{Li} are the SM left-handed doublets for quarks and leptons and χ_R is the right-handed component of the new fermion. Therefore, for model 3 we have

- A fermion singlet χ_R with charge -1;
- A coloured scalar doublet ϕ_3, with $\phi_3^T = \begin{bmatrix}\phi_q^{+5/3} & \phi_q^{+2/3}\end{bmatrix}$, where $\phi_3^{+5/3}$ and $\phi_3^{+2/3}$ are complex scalar fields with electric charge $+5/3$ and $+2/3$ respectively;

- A colourless scalar doublet ϕ_2, with $\phi_2^T = \left[\phi_I^{+1} \quad \frac{S+iA}{\sqrt{2}}\right]$, where ϕ_I^{+1} is a complex scalar field with charge $+1$ and we separated the lower component of the doublet in its real and imaginary parts S and A, which are real scalar fields with no charge and opposite CP parities;

while for model 5 we obtain

- A fermion doublet χ, with $\chi^T = (\chi^0, \chi^-)$, where χ^0 and χ^- are complex fermionic fields with electric charge 0 and -1 respectively;
- A coloured scalar singlet $\phi_3^{+2/3}$ with electric charge $+2/3$;
- A colourless neutral scalar singlet ϕ_2, which can be separated in its real and imaginary part as $\phi_2 = (S + iA)/\sqrt{2}$.

The SM and DM sectors also interact via the scalar potential. In model 3, where the scalars are $SU(2)_L$ doublets, the scalar potential is given by (with all parameters real)

$$\begin{aligned} V(H, \phi_I, \phi_q) = & - m_{11}|\phi_1|^2 + m_{22}|\phi_2|^2 + m_{33}|\phi_3|^2 + \lambda_1|\phi_1|^4 + \lambda_2|\phi_2|^4 - \lambda_3|\phi_{3,a}|^2|\phi_{3,b}|^2 + \\ & + \lambda_{12}|\phi_1|^2|\phi_2|^2 + \lambda_{13}|\phi_1|^2|\phi_3|^2 + \lambda_{23}|\phi_2|^2|\phi_3|^2 + \lambda_5[(\phi_1^\dagger\phi_2)^2 + (\phi_2^\dagger\phi_1)^2] \\ & + \lambda'_{12}(\phi_1^\dagger \cdot \phi_2)(\phi_2^\dagger \cdot \phi_1) + \lambda'_{13}(\phi_1^\dagger \cdot \phi_3)(\phi_3^\dagger \cdot \phi_1) + \lambda'_{23}(\phi_2^\dagger \cdot \phi_3)(\phi_3^\dagger \cdot \phi_2)p \\ & + y_{13}(\phi_3^\dagger \cdot \tau_2 \cdot \phi_1)(\phi_1^\dagger \cdot \tau_2 \cdot \phi_3) + y_{23}(\phi_3^\dagger \cdot \tau_2 \cdot \phi_2)(\phi_2^\dagger \cdot \tau_2 \cdot \phi_3)\,, \end{aligned} \tag{3.2}$$

where ϕ_1 is the usual Higgs field in unitary gauge $\phi_1^T \to \left[0 \quad \frac{v_H+h}{\sqrt{2}}\right]$, with v being the vacuum expectation value (vev) $v \approx 246$ GeV and h the SM Higgs field. Furthermore, σ_2 is the second Pauli matrix. Note that usually the colour indices in ϕ_3 are omitted and a summation over colour is implied, except for the term proportional to λ_3 where the colour indices may be different. One can notice that the potential 3.2 is equivalent to the Two-Higgs-Doublet model if we just consider ϕ_1 and ϕ_2 [94]. The remaining terms include the possibilities invariant under all symmetries when ϕ_3 is present.

The SM-Higgs-Doublet acquires a vev and we obtain a minimization condition of $m_{11}^2 = v^2\lambda_1$ and thus the scalar potential has 15 free parameters. We chose as the free input parameters of the potential the masses of the scalar fields and the quartic parameters λ_2, λ_3, λ_{12}, λ_{13}, λ_{23}, λ'_{23}, y_{13} and y_{23} are fixed by the W mass. Therefore, the following parameters were fixed

$$\lambda_1 = \frac{m_h^2}{2v^2} \qquad m_{22} = \frac{2m_{\phi_I}^2 - v^2\lambda_{12}}{2} \qquad m_{33}^2 = \frac{2m_{\phi_I^{+5/3}} - v^2 y_{13} - v^2\lambda_{13}}{2}\,, \tag{3.3}$$

$$\lambda_5 = \frac{m_S^2 - m_A^2}{2v^2} \qquad \lambda'_{12} = \frac{m_S^2 + m_A^2 - 2m_{\phi_I}^2}{v^2} \qquad \lambda'_{13} = \frac{2m_{\phi_q^{+2/3}} - 2m_{\phi_q^{+5/3}} + v^2 y_{13}}{v^2}\,, \tag{3.4}$$

where m_S, m_A, m_{ϕ_I} are the masses of the colourless scalars S, A and ϕ_I and $m_{\phi_q^{+5/3}}$, $m_{\phi_q^{+2/3}}$ are the masses of the coloured scalars $\phi_q^{+5/3}$, $\phi_q^{+2/3}$. Model 5 could have a fermionic candidate for DM. However, as discussed in [14], the direct detection constraints exclude this possibility due to tree-level Z mediation in DM-Nucleon scattering processes. The only way to avoid this limit is to push the fermion mass to be

of order $\mathcal{O}(TeV)$. This would in turn make the loop contributions to $b \to s\mu^+\mu^-$ and Δa_μ negligible and the flavour anomalies would remain unsolved. Therefore, the fermionic DM possibility is discarded in this case. In model 3, the fermion is charged and cannot be a DM candidate. Therefore, the DM candidate can only be one of the neutral components of ϕ_2, either S or A, similarly to what was done on the previous work [14]. Since the two DM candidates are identical in terms of DM and flavor phenomenology, we may assume that $M_S < M_A$ so that S comprises the whole DM density. This condition implies that $\lambda_{12} m_{11}/\lambda_1 < 0$.

Moreover, the Dirac mass of the fermion χ is given by the Lagrangean term $m_\chi \bar{\chi_L}\chi_R + h.c.$ and the Yukawa interaction 3.1 can be rewritten as

$$\mathcal{L} = y_{di}(\bar{u_{Lj}} V_{ji} \chi^- \phi_q^{+5/3} + \bar{d_{Li}}\chi^- \phi_q^{+2/3}) + y_{Li}\left(\bar{\nu_{Li}}\chi^-\phi_l^+ + \frac{e_{Li}}{\sqrt{2}}\chi^-(S+iA)\right) + h.c.\,, \tag{3.5}$$

where y_{di} are the coupling constants for the quarks in their mass eigenstates and V is the Cabibbo-Kobayashi-Maskawa (CKM) matrix. For simplicity, we only take y_b, y_s and y_μ to be non-zero.

Finally, since we introduced new particles to the SM, for model 3 we must also introduce the electroweak oblique parameters S, T and U [95, 96], which are able to quantify deviations from the SM due to corrections on the two-point functions using electroweak data [97]. Therefore, one can write for the total two point function

$$\Pi_{ab}(q^2) = \Pi_{ab}^{SM}(q^2) + \delta\Pi_{ab}(q^2)\,, \tag{3.6}$$

where a, b can be one of the gauge bosons γ, Z and $W^\pm$, q^2 is the external squared momentum and $\delta\Pi_{ab}$ is the new physics contributions. In model 5, the contributions for these parameters is zero because both fields are $SU(2)_L$ singlets and the two components in the doublet fermion χ have the same mass, leading to a vanishing to the electroweak oblique parameters at one-loop level. In this work we only considered the limits on the parameter T. The fermion χ has a vanishing contribution to T (because the fermion vacuum polarization diagram at one-loop is zero in the limit where the momentum goes to zero, similarly to what happens in QED). Therefore, the only contributions for the T parameter come from the scalar fields. Following [98], we considered a general expression for the parameter T with an arbitrary number of scalar doublets with hypercharge $\pm 1/2$ and scalar singlets. In model 3, if we just consider ϕ_1 and ϕ_2, this corresponds to a 2HDM with a dark doublet [94] where the NP contribution is given by [98]:

$$T = \frac{g^2}{64\pi^2 M_W^2 \alpha}[F(M_{\phi_l}^2, M_S^2) + F(M_{\phi_l}^2, M_A^2) - F(M_S^2, M_A^2)]\,, \tag{3.7}$$

where m_W is the mass of the $W^\pm$ gauge boson, α is the fine structure constant and g is the $SU(2)_L$ coupling constant. The function $F(A, B)$ is given by

$$F(A,B) = \begin{cases} \frac{A+B}{2} - \frac{AB}{A-B}\log\frac{A}{B} & , A \neq B \\ 0 & , A = B \end{cases}. \tag{3.8}$$

Similarly for ϕ_3, one can prove that the T parameter is proportional to $F((m_{\phi_q^{+5/3}})^2, (m_{\phi_q^{+2/3}})^2)$ and thus

vanishes, since the masses of these scalars are set to be equal. Note that the assumption of tree-level equality for the masses of the coloured scalars in Model 3 would be spoiled by the radiative corrections. In this case, the dominant contribution comes from the one-loop effect of the SM-like Higgs, which is of the order $(\lambda'_{13}v)^2/(4\pi)^2$. However, by fixing the coloured scalar masses to be around 1500 GeV, the mass difference from these corrections are always smaller than the tree-level mass by at least two orders of magnitude and thus the effects can be neglected. Therefore, the T parameter contribution only comes from the expression (3.7), with the limit being used $T = 0.03 \pm 0.12$, which will be applied at the end of the scan.

Chapter 4

Phenomenology

4.1 Flavour phenomenology

In this section we discuss the flavour constraints of the model. We must verify that not only we solve the discrepancies observed experimentally but also make sure that the observables in agreement with the SM predictions are not modified. Since the phenomenology is identical for both models, that is, both model 3 and model 5 have the same NP contributions to the relevant flavour observables, then we can use the same constraints and analytic expressions as in [14] for both models.

4.1.1 Anomalous moment of the muon $(g-2)_\mu$

We start by analysing the anomalous magnetic moment of the muon. In model 3, the leading order (LO) NP contribution comes from one-loop diagrams containing the fermion χ and the scalars S or A and we can write [99]

$$\Delta a_\mu = \frac{m_\mu^2 |y_\mu|^2}{16\pi^2 m_\chi^2}[\tilde{F}_7(x_S) + \tilde{F}_7(x_A)]\,, \tag{4.1}$$

with

$$\tilde{F}_7(x) = \frac{1 - 6x + 3x^2 + 2x^3 - 6x^2 log(x)}{12(1-x)^4} \tag{4.2}$$

and $x_{S(A)} = m_{S(A)}^2/m_\chi^2$.

4.1.2 $B \to K^* \mu^+ \mu^-$ decay

The effects of the loop transition $b \to s\mu^+\mu^-$ illustrated in figure 4.1 can be described using an effective field theory. For that, we generate an effective Hamiltonian for this new interaction given by [100, 101]

$$\mathcal{H}_{eff} = -\frac{4G_F}{\sqrt{2}} V_{tb} V_{ts}^* (C_9^{NP}\mathcal{O}_9 + C_{10}^{NP}\mathcal{O}_{10})\,, \tag{4.3}$$

where V_{tb} and V_{ts}^* are CKM matrix elements, C_9^{NP} and C_{10}^{NP} are the Wilson coefficients and $\mathcal{O}_9$, $\mathcal{O}_{10}$ are the following operators:

$$\mathcal{O}_9 = \frac{\alpha}{4\pi}[\bar{s}\gamma^\nu P_L b][\bar{\mu}\gamma_\nu \mu] \qquad \mathcal{O}_{10} = \frac{\alpha}{4\pi}[\bar{s}\gamma^\nu P_L b][\bar{\mu}\gamma_\nu\gamma_5 \mu]\,. \tag{4.4}$$

The main contribution to these operators comes from the box diagram in figure 4.1 and the respective Wilson coefficients are given by [14, 99]

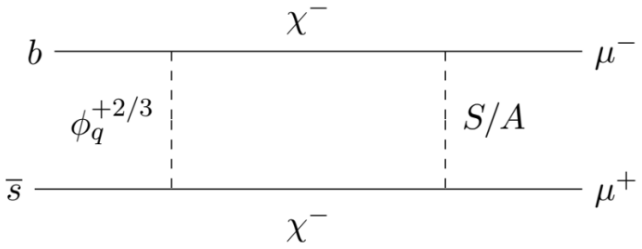

Figure 4.1: One-loop Feynman diagram to solve the $R(K^{(*)})$ anomalies.

$$C_9^{box} = -C_{10}^{box} = \mathcal{N}\frac{y_s y_b^* |y_\mu|^2}{64\pi\alpha m_\chi^2}[F(x_{\phi_q}, x_S) + F(x_{\phi_q}, x_A)] \tag{4.5}$$

with $\mathcal{N}^{-1} = \frac{4G_F V_{tb}V_{ts}^*}{\sqrt{2}}$, $x_{\phi_q,S,A} = \frac{m^2_{\phi_q,S,A}}{m^2_\chi}$ and

$$F(x,y) = \frac{1}{(1-x)(1-y)} + \frac{x^2 lnx}{(1-x)^2(x-y)} + \frac{y^2 lny}{(1-y)^2(y-x)}\,. \tag{4.6}$$

Considering the most recent experimental results, the best fitted values of the Wilson coefficients are $C_9^{NP} = -C_{10}^{NP} = [-0.59, -0.30]$ [102], with a 2σ confidence level and therefore in our scan we will consider the points in the parameter space that generate values of C_9^{NP} within the 2σ range of its central value.

4.1.3 $B_s - \bar{B}_s$ mixing

Another relevant constraint associated to the $b \to s$ transition comes from the $B_s - \bar{B}_s$ mixing, which consists on the phenomena where the B_s meson oscillates between its particle and antiparticle. Here, the only contribution arises from the effective operator

$$\mathcal{H}_{eff}^{B\bar{B}} = C_{B\bar{B}}(\bar{s_\alpha}\gamma^\mu P_L b_\alpha)(\bar{s_\beta}\gamma^\mu P_L b_\beta)\,, \tag{4.7}$$

where α and β denote the coloured indices. The NP contribution to the Wilson coefficient is given by [99]

$$C_{B\bar{B}}^{NP} = \frac{(y_s y_b^*)^2}{128\pi^2 m_\chi^2} F(x_{\phi_q}, x_{\phi_q})\,, \tag{4.8}$$

with

$$F(x,x) = \frac{1 - x^2 + 2x lnx}{(1-x)^3}\,. \tag{4.9}$$

The constraint is set on the mass difference ΔM_s of the two states B_s and $\bar{B}_s$. We can represent this constraint in terms of the ratio of the experimental and SM values for the mass difference, defining the quantity [103]:

$$R_{\Delta M_s} = \frac{\Delta M_s^{exp}}{\Delta M_s^{SM}} - 1 = -0.09 \pm 0.08 \quad at\ 1\sigma\ C.L.\,. \tag{4.10}$$

One can thus write $R_{\Delta M_s}^{exp}$ in terms of the NP and SM Wilson coefficients [103, 104]:

$$R_{\Delta M_s} = \left| 1 + \frac{0.8 C_{B\bar{B}}^{NP}(\mu_H)}{C_{B\bar{B}}^{SM}}(\mu_b) \right| - 1\,, \tag{4.11}$$

with $C_{B\bar{B}}^{NP}(\mu_H)$ being the NP Wilson coefficient at $\mu_H = 1TeV$ and $C_{B\bar{B}}^{SM}(\mu_b) \approx 7.2 \times 10^{-11} GeV^{-2}$ the corresponding SM value at the scale μ_b [105].

4.2 Dark Matter phenomenology

In this section we discuss the constraints arising from DM physics, taking into account DM relic density observations, constraints from DM direct detection and collider searches. The particle S is the chosen DM candidate. However, choosing A would lead to identical results since both particles have identical quantum numbers. Since S is a DM candidate, it must be able to reproduce the current DM relic abundance $\Omega_{DM}h^2 = 0.1199 \pm 0.0022$ [106]. We assume that the DM relic density is originated by a freeze-out mechanism and thus the number density of S n_S can be obtained through the Boltzmann equation

$$\frac{dn_S}{dt} + 3Hn_S = -\langle \sigma v \rangle \left(n_S^2 - n_{S_{eq}}^2 \right), \tag{4.12}$$

where $n_{S_{eq}}$ is the number density of S at equilibrium, H is the Hubble parameter and $\langle \sigma v \rangle$ is the thermally averaged DM annihilation cross section times its relative velocity. The Boltzmann equation (4.12) can be solved numerically using the software MICROMEGAS [107] which takes into account all possible DM annihilation and co-annihilation channels. The freeze-in mechanism, which is also a well-known alternative mechanism that explains DM abundance cannot be used in this case since our model requires very weak couplings between the DM particle and the visible sector $\mathcal{O}(10^{-10} - 10^{-12})$ [108].

An interesting aspect of model 3 is that, since the scalar fields are doublets, they can couple to the gauge bosons, unlike model 5 where the scalar fields are singlets. This will drastically change the distribution of the DM relic abundance. For model 3, the relevant annihilation and co-annihilation processes are present in figure 4.2 and 4.3 while for model 5 the processes are described by figures 4.4 and 4.5

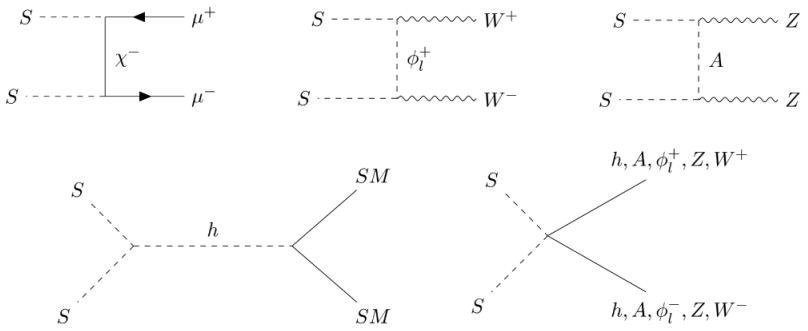

Figure 4.2: Diagrams for DM Annihilation in model 3; SM represents all SM massive particles.

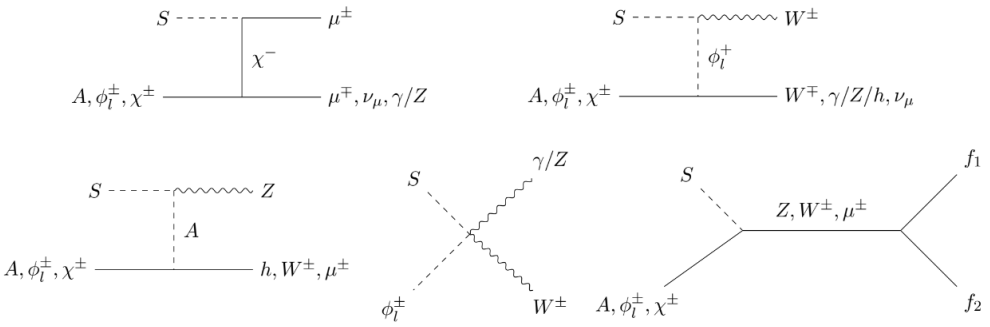

Figure 4.3: Diagrams for DM Co-annihilation in model 3; f_1, f_2 represent all possible SM final states of the s diagram.

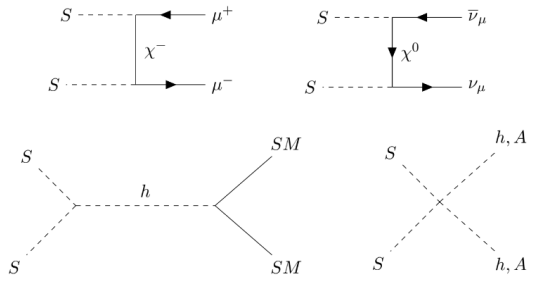

Figure 4.4: Diagrams for DM Annihilation in model 5.

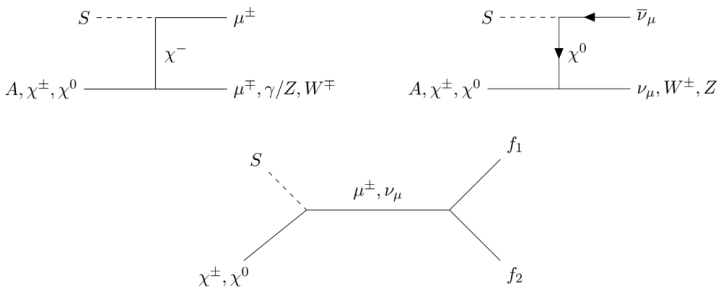

Figure 4.5: Diagrams for DM Co-annihilation in model 5; f_1, f_2 represent all possible SM final states of the s diagram.

Besides the relic density constraint, we must take into account DM direct detection (DD) results which may also place several constraints on the parameter space of model 3. Currently, the best experimental upper bounds on the DM direct detection cross section for a mass above 6 GeV are provided by the PandaX-4T [109] and the XENON1T [110] experiments. More recently, the LuxZeplin (LZ) experiment has also released their bounds on the spin independent cross section [111, 112]. We will show the three limits in our plots which will allow to understand the effect of future DD bounds. In model 3, the dominant DM DD channel is a tree-level t-channel with a Higgs-like mediation corresponding to the scattering process $SN \to SN$ (with N representing a nucleon), which has a cross section

$$\sigma(SN \to SN) = \frac{(\lambda_{12} + \lambda'_{12} + 2\lambda_5)^2}{4\pi} \frac{f_N^2 m_N^2 \mu_{SN}^2}{m_S^2 m_h^4}\,, \tag{4.13}$$

where $f_N \approx 0.3$ is an effective Higgs-nucleon coupling, m_N is the nucleon mass and μ_{SN} is the DM-nucleon reduced mass [113–116].

Another source of constraints to the model is the result of collider searches on DM at LHC, in particular the constraint of a SM-Higgs boson decaying into an S pair. For this decay, which is allowed when $m_S < m_h/2$, the width is given by

$$\Gamma(h \to SS) = \frac{(\lambda_{12} + \lambda'_{12} + 2\lambda_5)^2 v^2}{32\pi m_h} \sqrt{1 - \frac{4m_S^2}{m_h^2}} \tag{4.14}$$

and currently has an upper bound of 0.11 [5]. These are the DM searches constraints considered in this study. As we will see, the DM DD limit gives rise to a much stricter limit than the Higgs invisible width.

Finally, we discuss DM indirect detection bounds [117]. It was shown in Ref. [118] that, for the model parameter space of interest, the strongest upper bound for DM indirect searches is provided by the Fermi-LAT observations of gamma-ray signal in the dwarf spheroidal galaxies of the Milky Way [119]. However, the annihilation of scalar DM pairs in both models is dominated by the SM Higgs-mediated processes via the Higgs portal coupling (since the annihilation into $\mu^+\mu^-$ through the t/u-channel χ-exchange is d-wave suppressed). Thus, most DM indirect detection experiments only provide additional constraints on the Higgs portal coupling λ_{hS}, which is also directly constrained by the DM direct detection experiments. By scanning the parameter space for model 5 in Ref. [14], we have found that the DM direct searches like XENON1T, PandaX-4T and the latest LZ always give much more stringent upper bound on the Higgs portal coupling than the present DM indirect searches, so that we have not shown the Fermi-LAT upper bounds in our work. Moreover, since the Yukawa coupling of the DM scalar with the muon is quite large ($y_\mu \geq 1$), it is generically expected in Refs. [120, 121] that the two-to-three process $SS \to \mu\mu\gamma$ and the loop-induced one $SS \to \gamma\gamma$ should be visible by observing the sharp spectral features in the gamma-ray sky by Fermi-LAT [122] and HESS [123]. As shown in Figs. 11 and 12 of Ref. [121], except for the narrow regions near the Higgs resonance where the Higgs portal coupling dominates the DM freeze-out and around $m_S \sim 200GeV$ where the constraint becomes weaker, most benchmark parameters in model 5 would be well constrained since the correct DM relic abundance requires large Yukawa coupling y_μ to increase the cross section of $SS \to \mu^+\mu^-$. These gamma-ray spectral constraints

also apply to model 3 where the S co-annihilation by the χ-exchange channel to $\mu^+\mu^-$ during freeze-out also exists. However, in view of the large astrophysical and systematic uncertainties when looking for these DM indirect detection constraints, we do not use them in our numerical scanning of the models parameter space.

Chapter 5

Results

5.1 Initial scan setup

In this section, we discuss the results obtained for model 3 by performing a multi parameter scan taking into account the flavour and DM constraints mentioned before, in order to obtain the allowed parameter space for the model. The relevant parameters for Model 3 are

$$y_b, y_s, y_\mu, m_\chi, m_{\phi_q^{+5/3}}, m_{\phi_q^{+2/3}}, m_S, m_A, m_{\phi_l}, \lambda_{hS}, \lambda_2\,,$$

with $\lambda_{hS} = \lambda_{12} + \lambda'_{12} + 2\lambda_5$ being the Higgs portal coupling. It would be expected that the quartic parameters λ_{23}, λ'_{23} and y_{23} were also relevant, since they have an impact in the DM abundance through co-annihilation channels involving the coloured scalar fields. However, since there is a huge difference between the DM mass and masses of the coloured scalars [14], the contribution of these processes to the relic density will be very small. The values chosen for these parameters were $\lambda_{23} = \lambda'_{23} = y_{23} = 10^{-3}$. The parameters λ_3, λ_{13} and y_{13} are irrelevant for the discussion since they have no contribution for the DM and flavour physics.

The results are divided in two scans: In scan I (figures 5.1 and 5.2) our goal was to get a feel for the allowed parameter space of model 3 by varying its input parameters, while in scan II we fine-tuned the parameters taking into account the results from scan I in order to find points that satisfy all previously mentioned constraints. Therefore, the results from scan II are our final results. It is necessary to explain the meaning of each color of the points present in our figures: all points in the parameter space explain the B meson data within a 2σ confidence interval. The blue points furthermore explain the DM relic density value, the green points also satisfy XENON1T DM DD and collider searches constraints and the red points additionally satisfy the muon $(g-2)$ data within 3σ (that is, all constraints simultaneously).

Before analysing the results, we need to discuss some simplifications made and the allowed values considered for the parameter scan: following the reasoning of [14], in the flavour phenomenology expressions of the B meson decay and $B_s - \bar{B}_s$ mixing, the coupling constants y_s and y_b appear exclusively in the combination $y_s y_b^*$ and thus we assume they are real and proportional to each other, with $y_s = -y_b/4$.

The minus sign appears because the product must be negative in order to solve the measurements of $R(K)$. Moreover we set $|y_b| \leq 1$ for both scans, $0 \leq y_\mu \leq 4\pi$ (scan I) and $1 \leq y_\mu \leq 4\pi$ (scan II), where the condition $1 \leq y_\mu$ appears for optimization purposes. We also fix the masses of the coloured scalars at 1.5 TeV, similarly to model 5, and force all other dark sector particles to be heavier than the DM candidate S by at least 10 GeV (and at most 1 TeV) in both scans, considering 5 GeV$\leq M_S \leq 1$ TeV (scan I) which is the average WIMP mass range, and 5 GeV$\leq M_S \leq 100$ GeV (scan II), where the upper limit $m_S \leq 100$ GeV appears to optimize the scan, since for reasons we will explain ahead m_S is restricted to be below 80 GeV to satisfy the DM constraints. For the masses of the remaining scalars, we take 15 GeV$\leq m_A, m_{\phi_I} \leq 2$ TeV (scan I). In scan II however, we consider constraints from the precision data and LEP experiments of the W and Z boson widths. Additionally, for the decays $W^\pm \to S\phi_I^\pm, A\phi_I^\pm$ and $Z \to SA, \phi_I^+\phi_I^-$ to be kinematically forbidden, the following relations must be verified

$$m_S + m_{\phi_I} > m_W \qquad m_A + m_{\phi_I} > m_W \qquad m_S + m_A > m_Z \qquad 2m_{\phi_I} > Mm_Z\,. \tag{5.1}$$

Moreover, the process $e^+e^- \to \phi_I^+\phi_I^-$ also sets the limit $m_{\phi_I} > 70$ GeV [124]. We also exclude the region where simultaneously $m_S < 80$ GeV, $m_A < 100$ GeV and $m_A - m_S > 8$ GeV, since they would allow a visible di-jet or di-lepton signal [125]. Thus we have 100 GeV$\leq m_A \leq 1.1$ TeV and 70 GeV$\leq m_{\phi_I} \leq 1.1$ TeV in scan II. It turned out that the conditions 5.1 did not need to be imposed since they are automatically satisfied by the points which satisfy all constraints (red points). We also imposed $m_A \geq 100$ GeV since in scan I we concluded that $m_S \leq 80$ GeV (and $m_A - m_S > 8$ GeV is immediately satisfied by design). Furthermore, the masses m_S, m_A and m_{ϕ_I} should be such that λ'_{12} and λ_5 are smaller than the perturbative limit 4π (in both scans). For the vectorlike fermion χ, we set the lower limit 101.2 GeV$\leq m_\chi \leq 2$ TeV (scan I) and 101.2 GeV$\leq m_\chi \leq 1.1$ TeV (scan II), where the lower limit comes from LEP searches for unstable heavy vectorlike charged leptons [126]. More recent constraints from the LHC exist for vectorlike leptons, but they do not apply to our model since those searches assume that the vectorlike leptons couple to tau leptons [127], or have very small amounts of missing transverse energy, $\not{E}_T$, in the final states [128]. Regarding the Higgs portal coupling, we impose $|\lambda_{hS}| \leq 1$ (scan I), which is achieved by setting $10^{-5} \leq \lambda_{12} \leq 0.5$ and rejecting points where $\lambda_5 < -0.2$ and $|\lambda'_{12}| \geq 0.1$. As for scan II, we used $10^{-7} \leq |\lambda_{hS}| \leq 10^{-2}$, and $\lambda_{12}, |\lambda_5|, |\lambda'_{12}| \leq 4\pi$. Unlike in model 5 where the Higgs portal coupling is a completely free parameter, here it depends on the masses of S and ϕ_I and thus needs to be fine-tuned in order to be very small (this will be discussed in more detail ahead). Finally, we consider λ_2, whose only contribution is to the DM relic density through the channels $SS \to AA, \phi_I^+\phi_I^-$. We take $\lambda_2 = 10^{-5}$ in order to suppress the channel contribution to the relic abundance. Although we did not vary the value λ_2 in any of the scans, we checked that we can have points satisfying the Planck observations for much larger values of λ_2. A summary of the values used for each parameter in scans I and II is shown in Tables 5.1 and 5.2, respectively:

y_b	y_s	y_μ	$m_\chi(GeV)$	$m_{\phi_q^{+5/3}}, m_{\phi_q^{+2/3}}(GeV)$
$[-1, 1]$	$-y_b/4$	$1, 4\pi$	$[101.2, 1100]$	1500
$m_S(GeV)$	$m_A(GeV)$	$m_{\phi_l}(GeV)$	λ_{12}	λ_2
$[5, 1000]$	$[15, 2000]$	$[15, 2000]$	$[10^{-5}, 0.5]$	10^{-5}

Table 5.1: Input values for model 3 scan I. Additionally, we impose $|\lambda_{hS}| \leq 1$, which is achieved by considering $\lambda_5 < -0.2$ and $|\lambda'_{12}| \geq 0.1$.

y_b	y_s	y_μ	$m_\chi(GeV)$	$m_{\phi_q^{+5/3}}, m_{\phi_q^{+2/3}}(GeV)$
$[-1, 1]$	$-y_b/4$	$1, 4\pi$	$[101.2, 1100]$	1500
$m_S(GeV)$	$m_A(GeV)$	$m_{\phi_l}(GeV)$	λ_{12}	λ_2
$[5, 100]$	$[100, 1100]$	$[70, 1100]$	$\leq 4\pi$	10^{-5}

Table 5.2: Input values for model 3 scan II. Additionally, we impose $10^{-7} \leq |\lambda_{hS}| \leq 10^{-2}$, which is achieved by considering $\lambda_5, |\lambda'_{12}| \leq 4\pi$.

5.2 Model parameter space

In both models it was possible to find a region of the parameter space which satisfies all constraints. However, this region is different for both models, with the main difference being related to the DM relic density as a function of its mass, as it can be observed in figure 5.1:

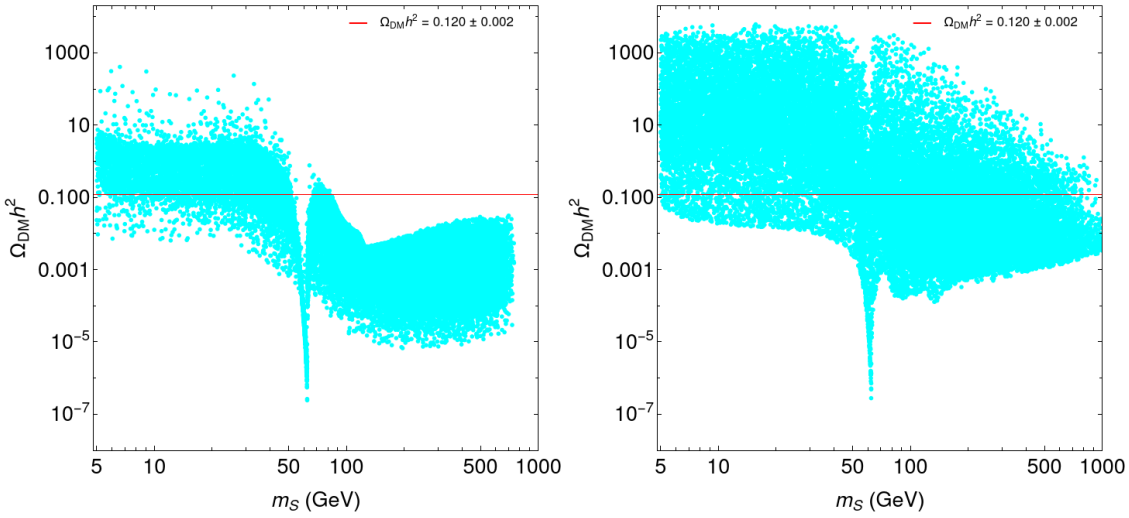

Figure 5.1: Scan I - DM relic density as a function of the DM mass for model 3 (left) and model 5 (right). The cyan points satisfy the B meson anomalies within a 2σ confidence value. The red line represents the observed DM relic density. For model 3, we also take $|\lambda_4| \leq 0.2$, $|\lambda_7| \leq 0.1$ and $|\lambda_{10}| \leq 0.5$. For model 5, the parameter values are the ones used in [14].

We immediately identify the same lower peak on both figures, around 60 GeV, which corresponds to the region of SM Higgs resonance $m_S \approx m_h/2$. In model 3, the DM mass has an upper limit of 80 GeV, while for model 5 no limit is observed. This result can be easily explained since the scalar fields in model 3 and model 5 have different $SU(2)_L$ representations: in model 5 the scalar fields are singlets

while in model 3 they are doublets and allowed to couple to gauge bosons. Therefore, in model 3 the DM annihilation processes $SS \to W^+W^-$ and $SS \to ZZ$ are allowed, which does not happen in model 5. Thus in model 3 the DM relic density is smaller than the value given by the Planck observation when $m_S \geq m_W$, similarly to what was observed for the i2HDM [129]. Another distinction between the models comes from the Higgs portal coupling: while in model 5 the λ_{hS} parameter can be as small as desired, in model 3 one has the relation

$$\lambda_{hS} = \lambda_{12} + \lambda'_{12} + 2\lambda_5 = \lambda_{12} + 2\frac{(M_S^2 - M_{\phi_I}^2)}{v^2}\,. \tag{5.2}$$

Therefore, to have small values of λ_{hS} (of $\mathcal{O}(10^{-2})$), which is a constraint required by the experimental upper bounds of the LZ, PandaX-4T and XENON1T experiment, the difference between the masses of S and ϕ_I must be small or else we must verify that λ_{12} is very close to $-2(m_S^2 - m_{\phi_I}^2)/v^2$. This condition is shown in figure 5.2:

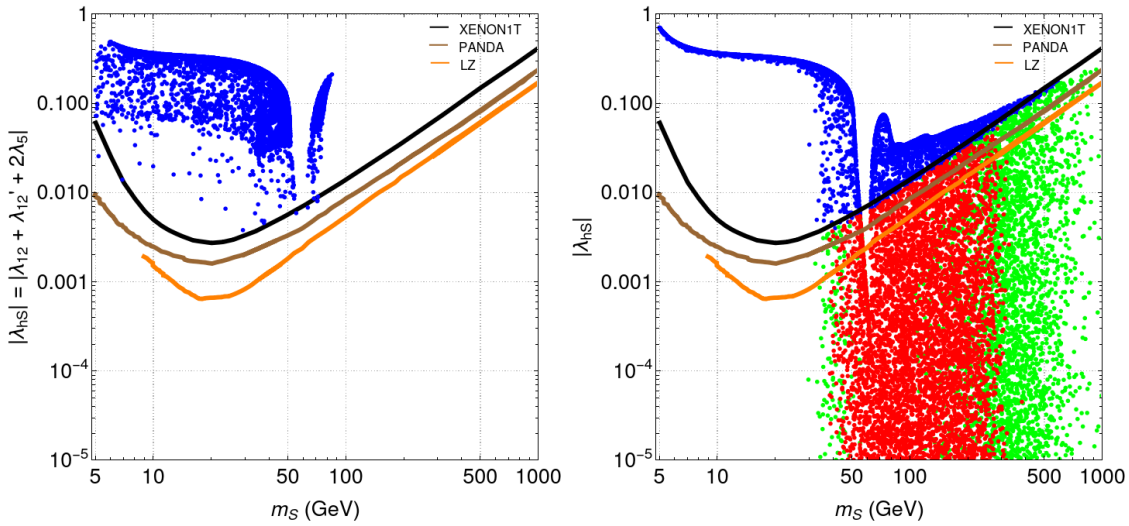

Figure 5.2: Scan I - Higgs portal coupling $|\lambda_{HSS}|$ as a function of the DM mass for model 3 (left) and model 5 (right). The solid black, brown and orange lines represent an experimental upper bound provided by the XENON1T, PANDAX-4T and LZ experiments respectively. The values used for the parameters in the models are the same as in figure 5.1.

As opposed to what we see in model 5, all points in model 3 are excluded due to DM DD and Higgs decay constraints. Since m_S varies between $[5, 1000]$ GeV and the minimum mass difference between S and other new particle is 10 GeV, then the quantity $\left|2\,(m_S^2 - m_{\phi_I}^2)/v^2\right|$ can only be as small as ≈ 0.0066 and therefore the condition $\lambda_{hS} \leq 10^{-2}$ is extremely unlikely to occur without forcing $\lambda_{12} \approx -2\,(m_S^2 - m_{\phi_I}^2)/v^2$ or $m_S - m_{\phi_I}$ to be smaller. We chose to keep λ_{hS} small since the other option would make the co-annihilation processes more efficient and affect the DM relic density. The main results for model 3 are present in figures 5.3, 5.4 and 5.5 (scan II):

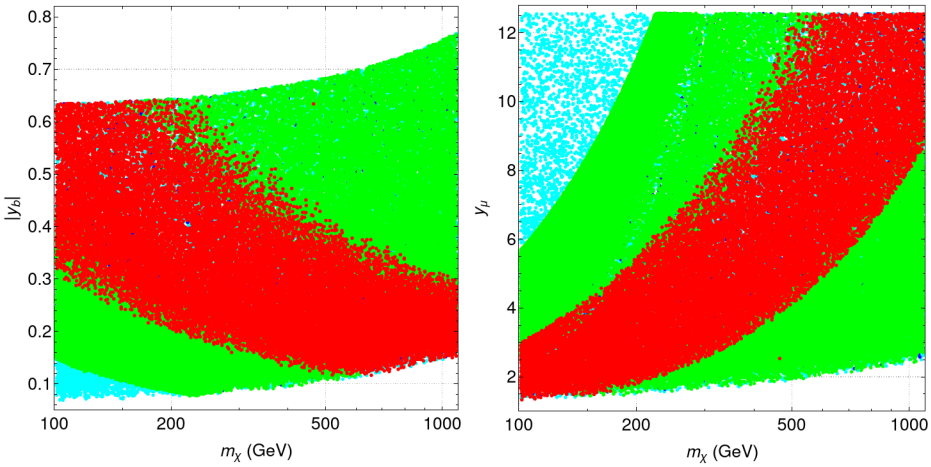

Figure 5.3: Scan II - Model 3 parameter space for $(|y_b|, M_\chi)$(left) and (y_μ, m_χ)(right) considering the parameter values $1 \leq y_\mu \leq 4\pi$, $10^{-7} \leq |\lambda_{HSS}| \leq 10^{-2}$ and $|\lambda_4|, |\lambda_7|, |\lambda_{10}| \leq 4\pi$.

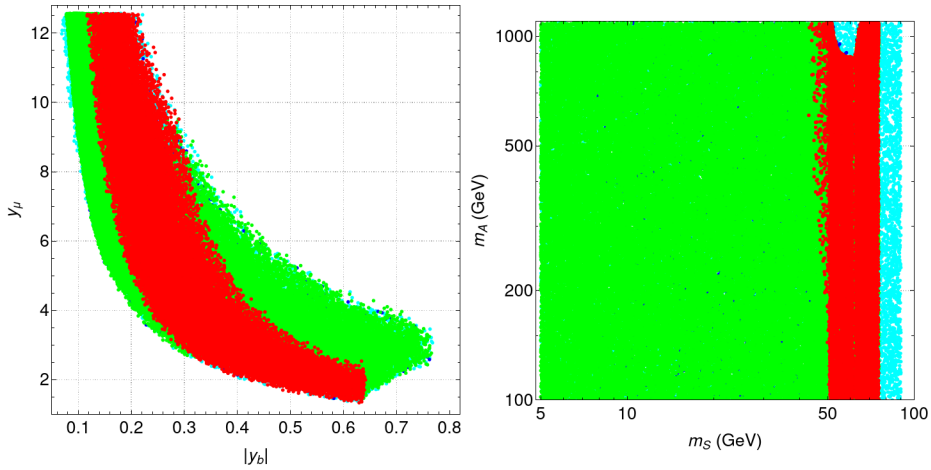

Figure 5.4: Scan II - Model 3 parameter space for $(y_\mu, |y_b|)$(left) and (m_A, m_S)(right).

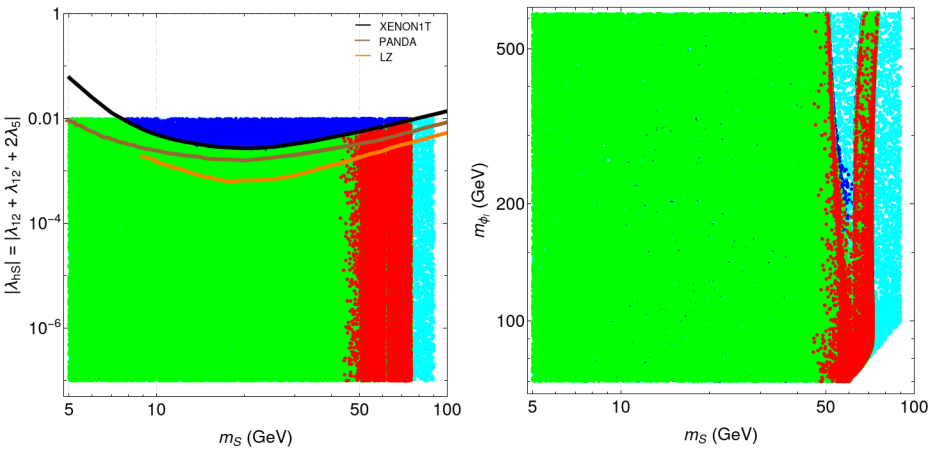

Figure 5.5: Scan II - Model 3 parameter space for $(|\lambda_{HSS}|, m_S)$(left) and (m_{ϕ_I}, m_S)(right). The solid black, brown and orange lines represent an experimental upper bound provided by the XENON1T, PANDAX-4T and LZ experiments respectively.

We see that the obtained results for the Yukawa couplings are similar to the ones in model 5, which was already expected since the flavour physics in both models is the same and the DM constraint do not have a big impact in the parameter space of these values. We obtained $|y_\mu| > 1.3$ and $0.11 \leq |y_b| \leq 0.65$ when all constraints are satisfied. We also note that, as we already saw in figure 5.1, the DM relic density limits the allowed value for the DM mass at $m_S < 80$ GeV. By further taking into account the $(g-2)$ constraint, we obtain 42 GeV$< m_S <$ 76 GeV, whereas in model 5 the allowed mass range was 30 GeV$< m_S <$ 350 GeV. This is a significant change in the allowed parameter space of the models: in model 3 the DM mass is limited in a very narrow range, while for model 5 the range is much wider. For the remaining parameters, we can observe in figure 5.4 that $M_A < 1076$ GeV. In figure 5.5, we present the bounds from the XENON1T, PandaX-4T and LZ and conclude that $m_{\phi_I} < 621$ GeV. The lower limit on m_{ϕ_I} was already expected since it is necessary to keep $\lambda_{12} < 4\pi$.

Afterwards, we applied the oblique T parameter to the allowed parameter space and obtained the following results, within a 2σ confidence value for the T parameter experimental bound:

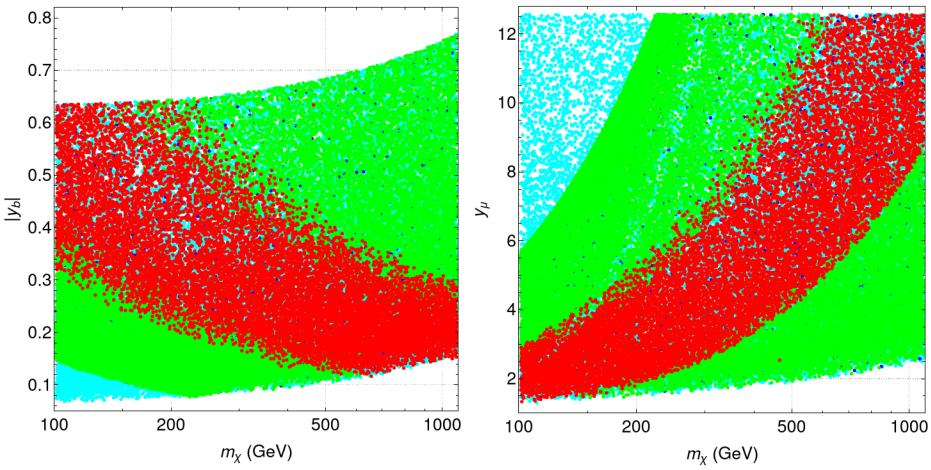

Figure 5.6: Model 3 parameter space for $(|y_b|, M_\chi)$(left) and (y_μ, M_χ)(right) after applying the T parameter limit.

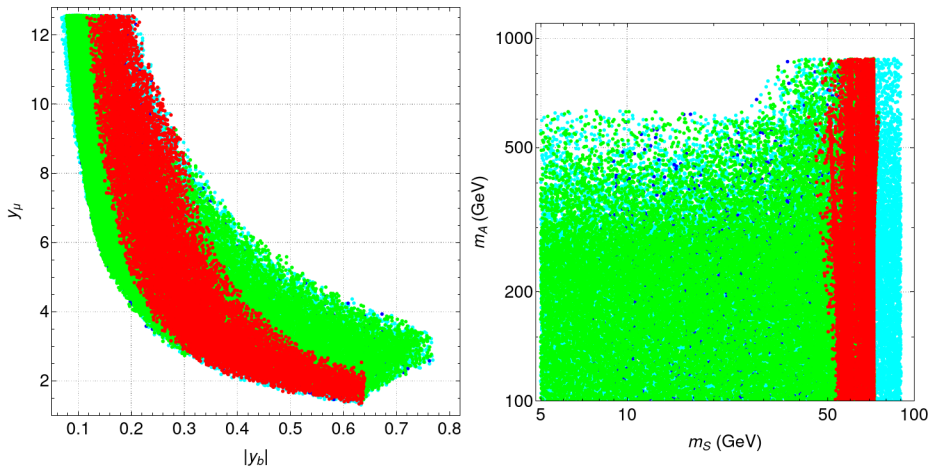

Figure 5.7: Model 3 parameter space for $(y_\mu, |y_b|)$(left) and (M_A, M_S)(right) after applying the T parameter limit.

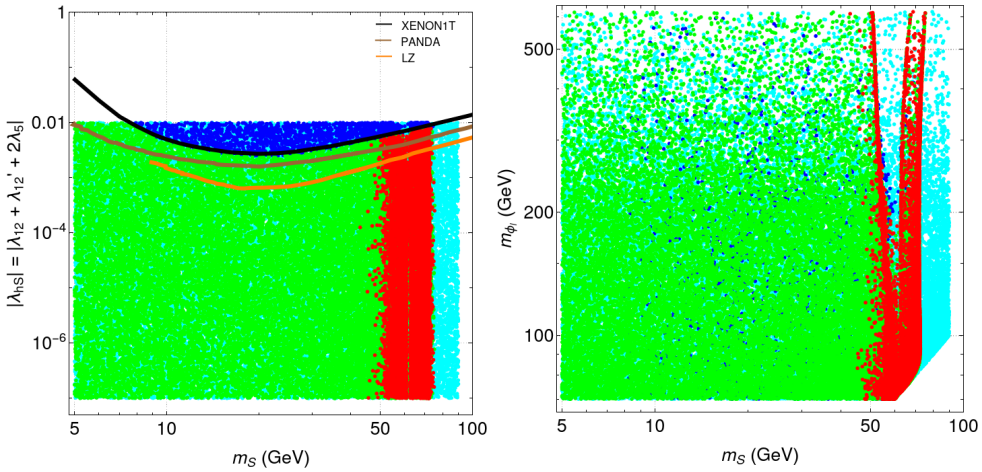

Figure 5.8: Model 3 parameter space for (λ_{HSS}, M_S)(left) and (M_{ϕ_I}, M_S)(right) after applying the T parameter limit.

We observe two major changes: the maximum allowed mass for A goes from 1076 GeV to 877 GeV, and for heavier masses ($m_{\phi_I} > 200$ GeV and $m_A > 300$ GeV), the vast majority of the allowed parameter space is now excluded. This is shown on figure 5.9, where now all points satisfy all previously mentioned constraints:

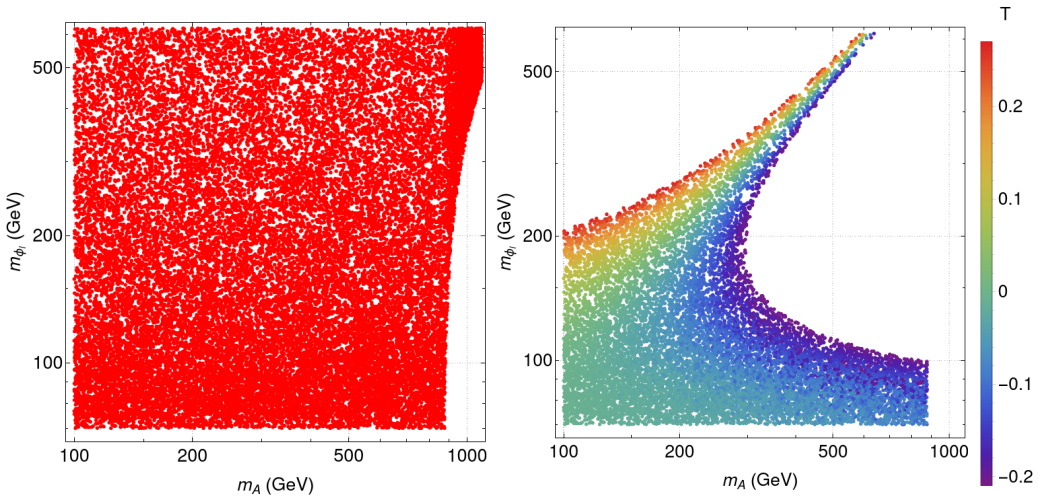

Figure 5.9: Model 3 parameter space for (M_{ϕ_I}, M_A) before applying the oblique parameter T limit(left) and after(right); The points presented here satisfy all constraints. The point color scheme on the right image describes different values for the T parameter.

As one can see on the right image in figure 5.9, the effects of the T parameter is to select regions close to the limit $m_{\phi_I} \approx m_A$, since this leads to $T \approx 0$. This is particularly true for large mass values $m_{\phi_I} > 200$ GeV. However, one can make the approximation $T \propto (m_{\phi_I} - m_A)/(m_{\phi_I} - m_S)$ [130] and thus significant mass splits can still be observed for small values of m_{ϕ_I}, where $m_{\phi_I} \approx m_S$. For larger values of M_{ϕ_I}, the only way to keep T in its experimental bound is to have $M_A \approx M_{\phi_I}$, which excludes a significant part of the parameter space in this region. Although only the T parameter was considered, the S parameter is not expected to affect greatly the model, since it only has a logarithmic dependence

on the mass split [129, 130].

5.3 Limits on y_μ

In this section we discuss the constraints on the y_μ coupling constant. The results on the previous sections (fig. 5.7) have shown the need for a sizeable Yukawa coupling ($y_\mu \geq 1$) of the dark-sector particles with the left-handed muons in order to explain the new physics results. As a consequence, both models could be further constrained by the measurement of muon-related observables sensitive to the new physics. As examples, let us consider the following diagrams:

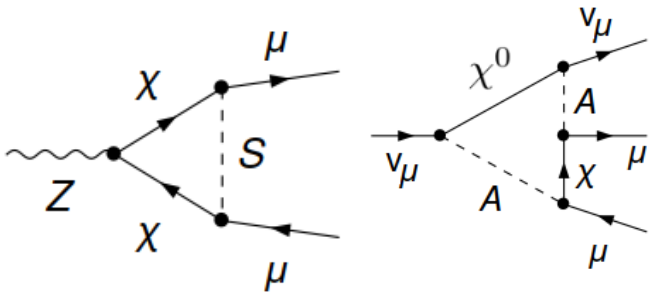

Figure 5.10: (Left) Diagram for the $Z \to \mu^+\mu^-$ decay with an amplitude $\propto |y_\mu|^2/(4\pi)^2$; (Right) Diagram for neutrino trident production with an amplitude $\propto |y_\mu|^4/(4\pi)^2$.

In the left case of 5.10, the Z_2-odd particles would shift the Z-boson coupling to the left-handed muons at one-loop level. This could potentially generate deviations in the decay width, the left-right polarization asymmetry and the forward-backward asymmetry of $Z \to \mu^+\mu^-$ at the Z-pole [5], which should be confronted with the precise measurements of these observables at LEP [131], Tevatron [132], and LHC [133–136]. Furthermore, similar one-loop diagrams would produce new corrections to the W-boson coupling with the muon-related charged current, which could potentially be detected by measuring the generalized Michel parameters [137, 138] in the radiative muon decay $\mu^- \to e^-\gamma\nu_\mu\bar{\nu}_e$ [5] or the associated tau decay $\tau^- \to \mu^-\gamma\nu_\tau\bar{\nu}_\mu$, with the latter process measured already precisely by ALEPH [139], CLEO [140], BABAR [141] and Belle [142]. Finally, both models would give rise to the new contributions to the muon neutrino trident production $\nu_\mu N \to \nu_\mu\mu^+\mu^- N$ [143, 144], which would be constrained by the data from CHARM-II [145], CCFR [146] and NuTeV [147] (a representative diagram is shown in the right plot of Figure 5.10). In the case $Z \to \mu^+\mu^-$ and in the muon/tau decays, the one-loop amplitudes are at most proportional to $|y_\mu|^2/(4\pi)^2)$ while in the case of neutrino trident production they are proportional to $|y_\mu|^4/(4\pi)^2$. In the neutrino trident case the diagrams are of the order:

$$\frac{|y_\mu|^4}{[4\pi \max(m_\chi, m_A)]^2} \leq \frac{|y_\mu|^4}{(4\pi m_\chi)^2}\,. \tag{5.3}$$

Hence, although the amplitude is enhanced by the fourth power of the Yukawa interaction, it is also suppressed by m_χ^2. As y_μ approaches 4π, m_χ tends to be closer to 1 TeV as can be seen in our fit 5.6. Given the large error bars in the associated experiments in the neutrino trident production, the constraint

on this one-loop correction should be rather weak and thus in most of the parameter space of interest, the constraints from these μ-related experiments are expected to be rather weak for both models.

Still, in order to understand how these constraints would affect the results if they were much larger than expected, we present the plots that are modified when the perturbative bounds are changed. We considered two scenarios besides the 4π bound, the conservative scenario, where we take $|y_\mu| \leq \sqrt{4\pi}$ and the ultra-conservative scenario with $|y_\mu| \leq \sqrt[4]{4\pi}$. In figure 5.11 we present, for Model 3, the allowed parameter space in the $((|y_b|, y_\mu)$ (left) and (m_χ, y_μ) (right) planes. All points verify all the previously imposed constraints with the red points having $|y_\mu| \leq 4\pi$, yellow points with $|y_\mu| \leq \sqrt{4\pi}$ and green points $|y_\mu| \leq \sqrt[4]{4\pi}$. The remaining plots are left unchanged:

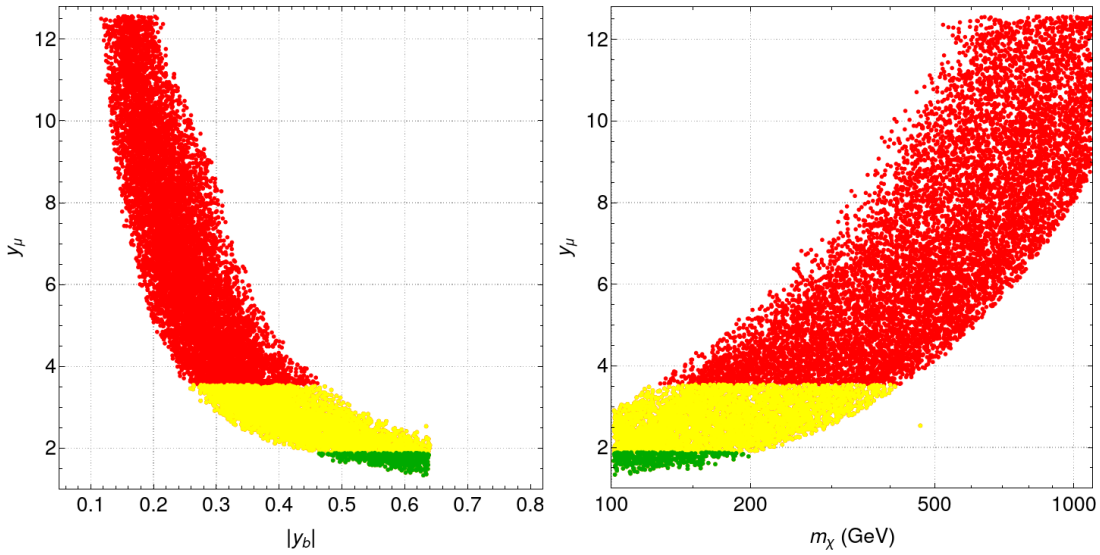

Figure 5.11: Model 3 parameter space in the $((|y_b|, y_\mu)$ (Left) and (m_χ, y_μ) (Right). All points verify all the previously imposed constraints with the red points having $|y_\mu| \leq 4\pi$, yellow points with $|y_\mu| \leq \sqrt{4\pi}$ and green points $|y_\mu| \leq \sqrt[4]{4\pi}$.

The main conclusion here is that the range of y_b and the χ mass is reduced but even in the very conservative scenario the model is still possible in a non-negligible slice of the parameter space.

5.4 Direct detection and the effect of future collider bounds

We finish this section by comparing the direct detection and collider bounds for future experiments. Recalling that the two observables are proportional to the portal coupling λ_{hS}, then the DD constraints act on the portal coupling as a function of the DM mass. In figure 5.12 we present the most recent DM DD bounds together with the LHC measurement of the Higgs invisible width for the $H \to SS$ process:

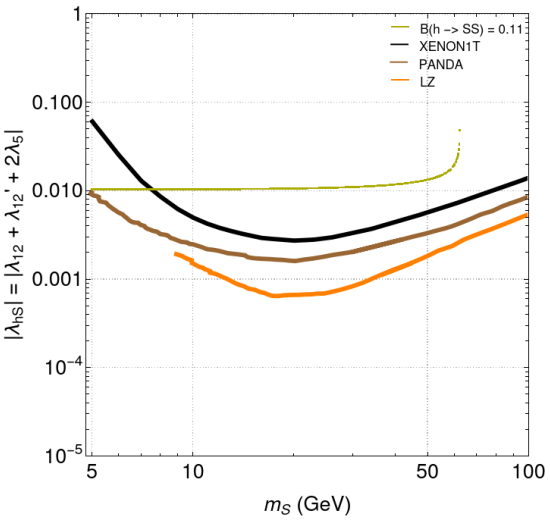

Figure 5.12: Comparison of the DM direct detection experiments using the measurements of the Higgs invisible width with the portal coupling as a function of the DM mass.

We observe that there is already more than one order of magnitude difference between the LZ experiment and the LHC measurement. Therefore, it is not expected that future measurements of the Higgs invisible width would be able to compete with direct detection experiments.

Chapter 6

Conclusions

We studied a model which provides a solution to the SM problem of lepton universality flavour violation in the $b \to s\mu^+\mu^-$ decay brought up by the LHCb and Belle collaborations. Additionally, this model also solves the muon $(g-2)$ anomaly and provides a DM candidate. In a previous work [14], a similar model was studied which differs from the present work in the group representation of the new dark sector scalar and fermion fields: in the previous model, the vector-like fermion χ was an $SU(2)_L$ doublet while the complex scalar fields ϕ_l and ϕ_q were $SU(2)_L$ singlets, with ϕ_q being an $SU(3)_c$ triplet. In this model, χ is an $SU(2)_L$ singlet while ϕ_l and ϕ_q are doublets.

We wanted to analyse how the different group representations affect the allowed parameter space of the models. The Yukawa Lagrangean for both models is such that the vertices present in the loop process which provides the NP results are identical, meaning that the contributions to the flavour observables and $(g-2)$ are the same. However, there are two major differences related to the DM observables: first, in order to explain the DM relic density value obtained by the Planck Collaboration, the DM mass must be lower than 80 GeV for model 3, whereas in model 5, this restriction does not exist. This is due to the fact that in Model 3, the DM scalar field can couple to the gauge bosons, which allows the annihilation processes $SS \to W^+W^-$ and $SS \to ZZ$ to occur, leading to a small relic density contribution. Second, there is a huge difference regarding the Higgs portal coupling. While in Model 5 this parameter is free, in Model 3 it is constrained and written as $\lambda_{HSS} = \lambda_{12} + 2(M_S^2 - M_{\phi_l}^2)/v^2$. To obtain a small constant, one must either choose λ_{12} and $2(M_S^2 - M_{\phi_l}^2)/v^2$ to be simultaneously small or $\lambda_{12} \approx -2(M_S^2 - M_{\phi_l}^2)/v^2$, with the latter one being the most viable option and the portal coupling values allowed to vary between 10^{-7} and 10^{-2}. The constraints coming from μ related experiments are expected to be weak for both models but could affect the parameter space for points close to the perturbative limit $y_\mu \approx 4\pi$.

In conclusion, the DM constraints are the ones acting on the models in a dramatically different manner. This difference is shown in the DM allowed mass range: while for model 5 the mass range was 30 GeV$< m_S <$ 350 GeV, here in model 3 the range is more restricted at 42 GeV$< m_S <$ 76 GeV. Over the last year, two new bounds from the DM direct detection experiments PANDAX-4T and LZ were released [111, 112]. Although by taking this into account the value of the portal coupling constant decreased, there were no changes on the allowed DM mass range.

The work developed on this thesis resulted in the writing of the scientific article [148].

Bibliography

[1] S. F. Novaes, Standard Model: An Introduction, **2000**.

[2] G. Aad, T. A. et. al, "Observation of a new particle in the search for the Standard Model Higgs boson with the ATLAS detector at the LHC", *Physics Letters B* **2012**, *716*, 1–29.

[3] M. E. Peskin, D. V. Schroeder, *An Introduction to quantum field theory*, Addison-Wesley, Reading, USA, **1995**.

[4] V. A. Bednyakov, N. D. Giokaris, A. V. Bednyakov, "On the Higgs mass generation mechanism in the Standard Model", *Physics of Particles and Nuclei* **2008**, *39*, 13–36.

[5] P. Zyla et al., "Review of Particle Physics", *PTEP* **2020**, *2020*, 083C01.

[6] S. Profumo, L. Giani, O. F. Piattella, An Introduction to Particle Dark Matter, **2019**.

[7] J. P. Ostriker, P. J. E. Peebles, A. Yahil, "The Size and Mass of Galaxies, and the Mass of the Universe", **1974**, *193*, L1.

[8] R. Spivey, "Planetary Heating by Neutrinos: Long-Term Habitats for Aquatic Life if Dark Energy Decays Favourably", *Journal of Modern Physics* **2013**, *4*, 20–47.

[9] G. R. Blumenthal, S. M. Faber, J. R. Primack, M. J. Rees, "Formation of galaxies and large-scale structure with cold dark matter.", **1984**, *311*, 517–525.

[10] P. J. E. Peebles, "Dark matter and the origin of galaxies and globular star clusters", **1984**, *277*, 470–477.

[11] J. Lewin, P. Smith, "Review of mathematics, numerical factors, and corrections for dark matter experiments based on elastic nuclear recoil", *Astroparticle Physics* **1996**, *6*, 87–112.

[12] S. Profumo, L. Giani, O. F. Piattella, An Introduction to Particle Dark Matter, **2019**.

[13] C. Alcock, R. A. A. et. al, "The MACHO Project: Microlensing Results from 5.7 Years of Large Magellanic Cloud Observations", *The Astrophysical Journal* **2000**, *542*, 281–307.

[14] D. Huang, A. P. Morais, R. Santos, "Anomalies in B-meson decays and the muon $g-2$ from dark loops", *Phys. Rev. D* **2020**, *102*, 075009.

[15] D. Coe, "Dark Matter Halo Mass Profiles", **2010**.

[16] J. Cooley, "Dark Matter direct detection of classical WIMPs", *SciPost Phys. Lect. Notes* **2022**, *55*, 1.

[17] M. Artuso, E. Barberio, S. Stone, "B Meson Decays", *PMC Phys. A* **2009**, *3*, 3.

[18] D. Hanneke, S. Fogwell Hoogerheide, G. Gabrielse, "Cavity control of a single-electron quantum cyclotron: Measuring the electron magnetic moment", *Phys. Rev. A* **2011**, *83*, 052122.

[19] A. Tewsley-Booth, The First Measurement of the Muon Anomalous Magnetic Moment from the Fermilab Muon $g-2$ Collaboration, **2022**.

[20] Z. Zhang, PhD thesis, Michigan U., **2018**.

[21] R. Aaij et al., "Test of lepton universality in beauty-quark decays", *Nature Phys.* **2022**, *18*, 277–282.

[22] R. Aaij et al., "Search for lepton-universality violation in $B^+ \to K^+\ell^+\ell^-$ decays", *Phys. Rev. Lett.* **2019**, *122*, 191801.

[23] R. Aaij et al., "Test of lepton universality with $B^0 \to K^{*0}\ell^+\ell^-$ decays", *JHEP* **2017**, *08*, 055.

[24] G. Hiller, F. Kruger, "More model-independent analysis of $b \to s$ processes", *Phys. Rev. D* **2004**, *69*, 074020.

[25] M. Bordone, G. Isidori, A. Pattori, "On the Standard Model predictions for R_K and R_{K^*}", *Eur. Phys. J. C* **2016**, *76*, 440.

[26] A. Abdesselam et al., "Test of Lepton-Flavor Universality in $B \to K^*\ell^+\ell^-$ Decays at Belle", *Phys. Rev. Lett.* **2021**, *126*, 161801.

[27] S. Choudhury et al., "Test of lepton flavor universality and search for lepton flavor violation in $B \to K\ell\ell$ decays", *JHEP* **2021**, *03*, 105.

[28] R. Aaij et al., "Differential branching fractions and isospin asymmetries of $B \to K^{(*)}\mu^+\mu^-$ decays", *JHEP* **2014**, *06*, 133.

[29] R. Aaij et al., "Angular analysis and differential branching fraction of the decay $B_s^0 \to \phi\mu^+\mu^-$", *JHEP* **2015**, *09*, 179.

[30] J. T. Wei et al., "Measurement of the Differential Branching Fraction and Forward-Backward Asymmetry for $B \to K^{(*)}\ell^+\ell^-$", *Phys. Rev. Lett.* **2009**, *103*, 171801.

[31] T. Aaltonen et al., "Measurements of the Angular Distributions in the Decays $B \to K^{(*)}\mu^+\mu^-$ at CDF", *Phys. Rev. Lett.* **2012**, *108*, 081807.

[32] V. Khachatryan et al., "Angular analysis of the decay $B^0 \to K^{*0}\mu^+\mu^-$ from pp collisions at $\sqrt{s} = 8$ TeV", *Phys. Lett. B* **2016**, *753*, 424–448.

[33] W. Adam, J. Pradler, J. Schieck, C. Schwanda, W. Waltenberger, Eds., Proceedings, LHCSki 2016 - A First Discussion of 13 TeV Results: Obergurgl, Austria, April 10-15, 2016, **2016**.

[34] J. P. Lees et al., "Measurement of angular asymmetries in the decays $B \to K^{*+-}$", *Phys. Rev. D* **2016**, *93*, 052015.

[35] R. Aaij et al., "Angular analysis of the $B^0 \to K^{*0}\mu^+\mu^-$ decay using 3 fb^{-1} of integrated luminosity", *JHEP* **2016**, *02*, 104.

[36] S. Wehle et al., "Lepton-Flavor-Dependent Angular Analysis of $B \to K^* \ell^+ \ell^-$", *Phys. Rev. Lett.* **2017**, *118*, 111801.

[37] A. M. Sirunyan et al., "Measurement of angular parameters from the decay $B^0 \to K^{*0} \mu^+ \mu^-$ in proton-proton collisions at $\sqrt{s} = 8$ TeV", *Phys. Lett. B* **2018**, *781*, 517–541.

[38] M. Aaboud et al., "Angular analysis of $B_d^0 \to K^* \mu^+ \mu^-$ decays in pp collisions at $\sqrt{s} = 8$ TeV with the ATLAS detector", *JHEP* **2018**, *10*, 047.

[39] A. J. Buras, J. Girrbach, "Left-handed Z' and Z FCNC quark couplings facing new $b \to s\mu^+\mu^-$ data", *JHEP* **2013**, *12*, 009.

[40] R. Gauld, F. Goertz, U. Haisch, "An explicit Z'-boson explanation of the $B \to K^* \mu^+ \mu^-$ anomaly", *JHEP* **2014**, *01*, 069.

[41] W. Altmannshofer, J. Davighi, M. Nardecchia, "Gauging the accidental symmetries of the standard model, and implications for the flavor anomalies", *Phys. Rev. D* **2020**, *101*, 015004.

[42] S. Lebbal, N. Mebarki, J. Mimouni, "Lepton Flavor Universality Violation in a 331 Model in $b \to s l^+ l^-$ Processes", **2020**.

[43] B. Capdevila, A. Crivellin, C. A. Manzari, M. Montull, "Explaining $b \to s\ell^+\ell^-$ and the Cabibbo angle anomaly with a vector triplet", *Phys. Rev. D* **2021**, *103*, 015032.

[44] M. Bauer, M. Neubert, "Minimal Leptoquark Explanation for the $R_{D^{(*)}}$, R_K , and $(g-2)_\mu$ Anomalies", *Phys. Rev. Lett.* **2016**, *116*, 141802.

[45] A. Angelescu, D. Bečirević, D. A. Faroughy, O. Sumensari, "Closing the window on single leptoquark solutions to the B-physics anomalies", *JHEP* **2018**, *10*, 183.

[46] A. Angelescu in 54th Rencontres de Moriond on Electroweak Interactions and Unified Theories, **2019**, pp. 309–314.

[47] S. Balaji, M. A. Schmidt, "Unified SU(4) theory for the $R_{D^{(*)}}$ and $R_{K^{(*)}}$ anomalies", *Phys. Rev. D* **2020**, *101*, 015026.

[48] A. Crivellin, D. Müller, F. Saturnino, "Flavor Phenomenology of the Leptoquark Singlet-Triplet Model", *JHEP* **2020**, *06*, 020.

[49] S. Saad, A. Thapa, "Common origin of neutrino masses and $R_{D^{(*)}}$, $R_{K^{(*)}}$ anomalies", *Phys. Rev. D* **2020**, *102*, 015014.

[50] J. Fuentes-Martín, P. Stangl, "Third-family quark-lepton unification with a fundamental composite Higgs", *Phys. Lett. B* **2020**, *811*, 135953.

[51] B. Capdevila, A. Crivellin, S. Descotes-Genon, J. Matias, J. Virto, "Patterns of New Physics in $b \to s\ell^+\ell^-$ transitions in the light of recent data", *JHEP* **2018**, *01*, 093.

[52] B. Gripaios, M. Nardecchia, S. A. Renner, "Linear flavour violation and anomalies in B physics", *JHEP* **2016**, *06*, 083.

[53] P. Arnan, L. Hofer, F. Mescia, A. Crivellin, "Loop effects of heavy new scalars and fermions in $b \to s\mu^+\mu^-$", *JHEP* **2017**, *04*, 043.

[54] P. Arnan, A. Crivellin, M. Fedele, F. Mescia, "Generic Loop Effects of New Scalars and Fermions in $b \to s\ell^+\ell^-$, $(g-2)_\mu$ and a Vector-like 4^{th} Generation", *JHEP* **2019**, *06*, 118.

[55] Q.-Y. Hu, L.-L. Huang, "Explaining $b \to s\ell^+\ell^-$ data by sneutrinos in the R -parity violating MSSM", *Phys. Rev. D* **2020**, *101*, 035030.

[56] Q.-Y. Hu, Y.-D. Yang, M.-D. Zheng, "Revisiting the B-physics anomalies in R-parity violating MSSM", *Eur. Phys. J. C* **2020**, *80*, 365.

[57] M. Tanabashi et al., "Review of Particle Physics", *Phys. Rev. D* **2018**, *98*, 030001.

[58] T. P. Gorringe, D. W. Hertzog, "Precision Muon Physics", *Prog. Part. Nucl. Phys.* **2015**, *84*, 73–123.

[59] T. Aoyama et al., "The anomalous magnetic moment of the muon in the Standard Model", *Phys. Rept.* **2020**, *887*, 1–166.

[60] B. Abi, A. et. al, "Measurement of the Positive Muon Anomalous Magnetic Moment to 0.46 ppm", *Phys. Rev. Lett.* **2021**, *126*, 141801.

[61] G. W. Bennett et al., "Final Report of the Muon E821 Anomalous Magnetic Moment Measurement at BNL", *Phys. Rev. D* **2006**, *73*, 072003.

[62] N. Saito, "A novel precision measurement of muon g-2 and EDM at J-PARC", *AIP Conf. Proc.* **2012**, *1467*, (Eds.: T. Fukuyama, R. N. Mohapatra), 45–56.

[63] J. Grange et al., "Muon (g-2) Technical Design Report", **2015**.

[64] A. Vicente, "Anomalies in $b \to s$ transitions and dark matter", *Adv. High Energy Phys.* **2018**, *2018*, 3905848.

[65] D. Aristizabal Sierra, F. Staub, A. Vicente, "Shedding light on the $b \to s$ anomalies with a dark sector", *Phys. Rev. D* **2015**, *92*, 015001.

[66] G. Bélanger, C. Delaunay, S. Westhoff, "A Dark Matter Relic From Muon Anomalies", *Phys. Rev. D* **2015**, *92*, 055021.

[67] W. Altmannshofer, S. Gori, S. Profumo, F. S. Queiroz, "Explaining dark matter and B decay anomalies with an $L_\mu - L_\tau$ model", *JHEP* **2016**, *12*, 106.

[68] A. Celis, W.-Z. Feng, M. Vollmann, "Dirac dark matter and $b \to s\ell^+\ell^-$ with $\mathrm{U}(1)$ gauge symmetry", *Phys. Rev. D* **2017**, *95*, 035018.

[69] J. M. Cline, J. M. Cornell, D. London, R. Watanabe, "Hidden sector explanation of B-decay and cosmic ray anomalies", *Phys. Rev. D* **2017**, *95*, 095015.

[70] J. Ellis, M. Fairbairn, P. Tunney, "Anomaly-Free Models for Flavour Anomalies", *Eur. Phys. J. C* **2018**, *78*, 238.

[71] S. Baek, "Dark matter contribution to $b \to s\mu^+\mu^-$ anomaly in local $U(1)_{L_\mu - L_\tau}$ model", *Phys. Lett. B* **2018**, *781*, 376–382.

[72] K. Fuyuto, H.-L. Li, J.-H. Yu, "Implications of hidden gauged $U(1)$ model for B anomalies", *Phys. Rev. D* **2018**, *97*, 115003.

[73] P. Cox, C. Han, T. T. Yanagida, "Right-handed Neutrino Dark Matter in a U(1) Extension of the Standard Model", *JCAP* **2018**, *01*, 029.

[74] A. Falkowski, S. F. King, E. Perdomo, M. Pierre, "Flavourful Z' portal for vector-like neutrino Dark Matter and $R_{K^{(*)}}$", *JHEP* **2018**, *08*, 061.

[75] L. Darmé, K. Kowalska, L. Roszkowski, E. M. Sessolo, "Flavor anomalies and dark matter in SUSY with an extra U(1)", *JHEP* **2018**, *10*, 052.

[76] S. Singirala, S. Sahoo, R. Mohanta, "Exploring dark matter, neutrino mass and $R_{K^{(*)},\phi}$ anomalies in $L_\mu - L_\tau$ model", *Phys. Rev. D* **2019**, *99*, 035042.

[77] S. Baek, C. Yu, "Dark matter for $b \to s\mu^+\mu^-$ anomaly in a gauged $U(1)_X$ model", *JHEP* **2018**, *11*, 054.

[78] A. Kamada, M. Yamada, T. T. Yanagida, "Self-interacting dark matter with a vector mediator: kinetic mixing with the $\mathrm{U}(1)_{(B-L)_3}$ gauge boson", *JHEP* **2019**, *03*, 021.

[79] D. Guadagnoli, M. Reboud, P. Stangl, "The Dark Side of 4321", *JHEP* **2020**, *10*, 084.

[80] I. de Medeiros Varzielas, O. Fischer, "Non-Abelian family symmetries as portals to dark matter", *JHEP* **2016**, *01*, 160.

[81] J. M. Cline, "B decay anomalies and dark matter from vectorlike confinement", *Phys. Rev. D* **2018**, *97*, 015013.

[82] C. Hati, G. Kumar, J. Orloff, A. M. Teixeira, "Reconciling B-meson decay anomalies with neutrino masses, dark matter and constraints from flavour violation", *JHEP* **2018**, *11*, 011.

[83] S.-M. Choi, Y.-J. Kang, H. M. Lee, T.-G. Ro, "Lepto-Quark Portal Dark Matter", *JHEP* **2018**, *10*, 104.

[84] A. Datta, J. L. Feng, S. Kamali, J. Kumar, "Resolving the $(g-2)_\mu$ and B Anomalies with Lepto-quarks and a Dark Higgs Boson", *Phys. Rev. D* **2020**, *101*, 035010.

[85] G. Belanger et al., "Leptoquark manoeuvres in the dark: a simultaneous solution of the dark matter problem and the $R_{D^{(*)}}$ anomalies", *JHEP* **2022**, *02*, 042.

[86] M. J. Baker, D. A. Faroughy, S. Trifinopoulos, "Collider signatures of coannihilating dark matter in light of the B-physics anomalies", *JHEP* **2021**, *11*, 084.

[87] A. Crivellin, M. Hoferichter, "Consequences of chirally enhanced explanations of (g $-$ 2) for h $\to$ $\mu\mu$ and Z $\to$ $\mu\mu$", *JHEP* **2021**, *07*, 135.

[88] B. Bhattacharya, D. London, J. M. Cline, A. Datta, G. Dupuis, "Quark-flavored scalar dark matter", *Phys. Rev. D* **2015**, *92*, 115012.

[89] J. Kawamura, S. Okawa, Y. Omura, "Interplay between the b$\to$ $s\ell\ell$ anomalies and dark matter physics", *Phys. Rev. D* **2017**, *96*, 075041.

[90] J. M. Cline, J. M. Cornell, "$R(K^{(*)})$ from dark matter exchange", *Phys. Lett. B* **2018**, *782*, 232–237.

[91] D. G. Cerdeño, A. Cheek, P. Martín-Ramiro, J. M. Moreno, "B anomalies and dark matter: a complex connection", *Eur. Phys. J. C* **2019**, *79*, 517.

[92] B. Barman, D. Borah, L. Mukherjee, S. Nandi, "Correlating the anomalous results in $b \to s$ decays with inert Higgs doublet dark matter and muon $(g-2)$", *Phys. Rev. D* **2019**, *100*, 115010.

[93] L. Darmé, M. Fedele, K. Kowalska, E. M. Sessolo, "Flavour anomalies from a split dark sector", *JHEP* **2020**, *08*, 148.

[94] E. Ma, "Verifiable radiative seesaw mechanism of neutrino mass and dark matter", *Phys. Rev. D* **2006**, *73*, 077301.

[95] M. E. Peskin, T. Takeuchi, "New constraint on a strongly interacting Higgs sector", *Phys. Rev. Lett.* **1990**, *65*, 964–967.

[96] M. E. Peskin, T. Takeuchi, "Estimation of oblique electroweak corrections", *Phys. Rev. D* **1992**, *46*, 381–409.

[97] G. Funk, D. O'Neil, R. M. Winters, "What the Oblique Parameters S, T, and U and Their Extensions Reveal About the 2HDM: A Numerical Analysis", *Int. J. Mod. Phys. A* **2012**, *27*, 1250021.

[98] W Grimus, L Lavoura, O. M. Ogreid, P Osland, "A precision constraint on multi-Higgs-doublet models", *Journal of Physics G: Nuclear and Particle Physics* **2008**, *35*, 075001.

[99] P. Arnan, L. Hofer, F. Mescia, A. Crivellin, "Loop effects of heavy new scalars and fermions in $b \to s\mu^+\mu^-$", *JHEP* **2017**, *04*, 043.

[100] W. Altmannshofer, P. Ball, A. Bharucha, A. J. Buras, D. M. Straub, M. Wick, "Symmetries and asymmetries of $B \to K\mu^+\mu^-$ decays in the Standard Model and beyond", *Journal of High Energy Physics* **2009**, *2009*, 019–019.

[101] E. e. a. Schneider, "Complementarity of the constraints on new physics from $B_s \to \mu^+\mu^-$ and from $B \to K\ell^+\ell^-$ decays", *Phys. Rev. D* **2012**, *86*, 034034.

[102] M. Algueró, B. Capdevila, S. Descotes-Genon, J. Matias, M. Novoa-Brunet, "$b \to s\ell^+\ell^-$ global fits after R_{K_S} and $R_{K^{*+}}$", *Eur. Phys. J. C* **2022**, *82*, 326.

[103] P. Arnan, A. Crivellin, M. Fedele, F. Mescia, Generic Loop Effects of New Scalars and Fermions in $b \to s\ell^+\ell^-$, $(g-2)_\mu$ and a Vector-like 4^{th} Generation, **2021**.

[104] F. Gabbiani, E. Gabrielli, A. Masiero, L. Silvestrini, "A complete analysis of FCNC and CP constraints in general SUSY extensions of the standard model", *Nuclear Physics B* **1996**, *477*, 321–352.

[105] A. Bazavov, B. et. al, "$B^0_{(s)}$-mixing matrix elements from lattice QCD for the Standard Model and beyond", *Phys. Rev. D* **2016**, *93*, 113016.

[106] Planck Collaboration, Aghanim, N.and Fernandez-Cobos, R. et. al, "Planck 2018 results - VI. Cosmological parameters", *A&A* **2020**, *641*, A6.

[107] G. Belanger, A. Mjallal, A. Pukhov, "Recasting direct detection limits within micrOMEGAs and implication for non-standard Dark Matter scenarios", *Eur. Phys. J. C* **2021**, *81*, 239.

[108] G. Bélanger, F. Boudjema, A. Goudelis, A. Pukhov, B. Zaldívar, "micrOMEGAs5.0: Freeze-in", *Computer Physics Communications* **2018**, *231*, 173–186.

[109] Y. Meng et al., "Dark Matter Search Results from the PandaX-4T Commissioning Run", *Phys. Rev. Lett.* **2021**, *127*, 261802.

[110] E. Aprile, A. et. al, "Dark Matter Search Results from a One Ton-Year Exposure of XENON1T", *Phys. Rev. Lett.* **2018**, *121*, 111302.

[111] D. S. Akerib et al., "Projected sensitivities of the LUX-ZEPLIN experiment to new physics via low-energy electron recoils", *Phys. Rev. D* **2021**, *104*, 092009.

[112] LZ collaboration, First Dark Matter Search Results from the LUX-ZEPLIN (LZ) Experiment, **2022**.

[113] J. M. Cline, P. Scott, K. Kainulainen, C. Weniger, "Update on scalar singlet dark matter", *Phys. Rev. D* **2013**, *88*, 055025.

[114] J. M. Alarcón, J. M. Camalich, J. A. Oller, "Chiral representation of the πN scattering amplitude and the pion-nucleon sigma term", *Phys. Rev. D* **2012**, *85*, 051503.

[115] X.-L. Ren, X.-Z. Ling, L.-S. Geng, "Pion–nucleon sigma term revisited in covariant baryon chiral perturbation theory", *Physics Letters B* **2018**, *783*, 7–12.

[116] M. Hoferichter, P. Klos, J. Menéndez, A. Schwenk, "Improved limits for Higgs-portal dark matter from LHC searches", *Phys. Rev. Lett.* **2017**, *119*, 181803.

[117] J. L. Feng, "Dark Matter Candidates from Particle Physics and Methods of Detection", *Ann. Rev. Astron. Astrophys.* **2010**, *48*, 495–545.

[118] G. Elor, N. L. Rodd, T. R. Slatyer, W. Xue, "Model-Independent Indirect Detection Constraints on Hidden Sector Dark Matter", *JCAP* **2016**, *06*, 024.

[119] M. Ackermann et al., "Searching for Dark Matter Annihilation from Milky Way Dwarf Spheroidal Galaxies with Six Years of Fermi Large Area Telescope Data", *Phys. Rev. Lett.* **2015**, *115*, 231301.

[120] F. Giacchino, L. Lopez-Honorez, M. H. G. Tytgat, "Scalar Dark Matter Models with Significant Internal Bremsstrahlung", *JCAP* **2013**, *10*, 025.

[121] A. Ibarra, T. Toma, M. Totzauer, S. Wild, "Sharp Gamma-ray Spectral Features from Scalar Dark Matter Annihilations", *Phys. Rev. D* **2014**, *90*, 043526.

[122] M. Ackermann et al., "Search for Gamma-ray Spectral Lines with the Fermi Large Area Telescope and Dark Matter Implications", *Phys. Rev. D* **2013**, *88*, 082002.

[123] A. Abramowski et al., "Search for Photon-Linelike Signatures from Dark Matter Annihilations with H.E.S.S.", *Phys. Rev. Lett.* **2013**, *110*, 041301.

[124] A. Pierce, J. Thaler, "Natural Dark Matter from an unnatural Higgs boson and new colored particles at the TeV scale", *Journal of High Energy Physics* **2007**, *2007*, 026–026.

[125] E. Lundstrom, M. Gustafsson, J. Edsjo, "The Inert Doublet Model and LEP II Limits", *Phys. Rev. D* **2009**, *79*, 035013.

[126] P. A. et. al, "Search for heavy neutral and charged leptons in e+e annihilation at LEP", *Physics Letters B* **2001**, *517*, 75–85.

[127] A. M. Sirunyan et al., "Search for vector-like leptons in multilepton final states in proton-proton collisions at $\sqrt{s}$ = 13 TeV", *Phys. Rev. D* **2019**, *100*, 052003.

[128] S. Bißmann, G. Hiller, C. Hormigos-Feliu, D. F. Litim, "Multi-lepton signatures of vector-like leptons with flavor", *Eur. Phys. J. C* **2021**, *81*, 101.

[129] A. Belyaev, G. Cacciapaglia, I. P. Ivanov, F. Rojas-Abatte, M. Thomas, "Anatomy of the Inert Two Higgs Doublet Model in the light of the LHC and non-LHC Dark Matter Searches", *Phys. Rev. D* **2018**, *97*, 035011.

[130] R. Barbieri, L. J. Hall, V. S. Rychkov, "Improved naturalness with a heavy Higgs: An Alternative road to LHC physics", *Phys. Rev. D* **2006**, *74*, 015007.

[131] S. Schael et al., "Precision electroweak measurements on the Z resonance", *Phys. Rept.* **2006**, *427*, 257–454.

[132] T. A. Aaltonen et al., "Tevatron Run II combination of the effective leptonic electroweak mixing angle", *Phys. Rev. D* **2018**, *97*, 112007.

[133] G. Aad et al., "Measurement of the forward-backward asymmetry of electron and muon pair-production in pp collisions at $\sqrt{s}$ = 7 TeV with the ATLAS detector", *JHEP* **2015**, *09*, 049.

[134] "Measurement of the effective leptonic weak mixing angle using electron and muon pairs from Z-boson decay in the ATLAS experiment at $\sqrt{s} = 8$ TeV", **2018**.

[135] A. M. Sirunyan et al., "Measurement of the weak mixing angle using the forward-backward asymmetry of Drell-Yan events in pp collisions at 8 TeV", *Eur. Phys. J. C* **2018**, *78*, 701.

[136] R. Aaij et al., "Measurement of the forward-backward asymmetry in $Z/\gamma^* \to \mu^+\mu^-$ decays and determination of the effective weak mixing angle", *JHEP* **2015**, *11*, 190.

[137] L. Michel, "Interaction between four half spin particles and the decay of the μ meson", *Proc. Phys. Soc. A* **1950**, *63*, (Eds.: T. Damour, I. Todorov, B. Zhilinskii), 514–531.

[138] C. Bouchiat, L. Michel, "Theory of μ-Meson Decay with the Hypothesis of Nonconservation of Parity", *Phys. Rev.* **1957**, *106*, (Eds.: T. Damour, I. Todorov, B. Zhilinskii), 170–172.

[139] A. Heister et al., "Measurement of the Michel parameters and the nu/tau helicity in tau lepton decays", *Eur. Phys. J. C* **2001**, *22*, 217–230.

[140] J. P. Alexander et al., "Determination of the Michel parameters and the tau-neutrino helicity in tau decay", *Phys. Rev. D* **1997**, *56*, 5320–5329.

[141] J. P. Lees et al., "Measurement of the branching fractions of the radiative leptonic τ decays $\tau \to e\gamma\nu\bar{\nu}$ and $\tau \to \mu\gamma\nu\bar{\nu}$ at *BABAR*", *Phys. Rev. D* **2015**, *91*, 051103.

[142] N. Shimizu et al., "Measurement of the tau Michel parameters $\bar{\eta}$ and $\xi\kappa$ in the radiative leptonic decay $\tau^- \to \ell^-\nu_\tau\bar{\nu}_\ell\gamma$", *PTEP* **2018**, *2018*, 023C01.

[143] W. Altmannshofer, S. Gori, M. Pospelov, I. Yavin, "Neutrino Trident Production: A Powerful Probe of New Physics with Neutrino Beams", *Phys. Rev. Lett.* **2014**, *113*, 091801.

[144] W. Altmannshofer, S. Gori, M. Pospelov, I. Yavin, "Quark flavor transitions in $L_\mu - L_\tau$ models", *Phys. Rev. D* **2014**, *89*, 095033.

[145] D. Geiregat et al., "First observation of neutrino trident production", *Phys. Lett. B* **1990**, *245*, 271–275.

[146] S. R. Mishra et al., "Neutrino tridents and W Z interference", *Phys. Rev. Lett.* **1991**, *66*, 3117–3120.

[147] T. Adams et al., "Evidence for diffractive charm production in muon-neutrino Fe and anti-muon-neutrino Fe scattering at the Tevatron", *Phys. Rev. D* **2000**, *61*, 092001.

[148] R. Capucha, D. Huang, T. Lopes, R. Santos, Impact of electroweak group representation in models for B and $g-2$ anomalies from Dark Loops, **2022**.

[149] R. Aaij et al., "Tests of lepton universality using $B^0 \to K^0_S \ell^+ \ell^-$ and $B^+ \to K^{*+} \ell^+ \ell^-$ decays", *Phys. Rev. Lett.* **2022**, *128*, 191802.

[150] G. Bertone, D. Hooper, "History of dark matter", *Rev. Mod. Phys.* **2018**, *90*, 045002.

[151] A. Crivellin, B. Fuks, L. Schnell, "Explaining the hints for lepton flavour universality violation with three S_2 leptoquark generations", **2022**.

[152] B. Abi et al., "Measurement of the Positive Muon Anomalous Magnetic Moment to 0.46 ppm", *Phys. Rev. Lett.* **2021**, *126*, 141801.

[153] P. A. R. Ade et al., "Planck 2015 results. XIII. Cosmological parameters", *Astron. Astrophys.* **2016**, *594*, A13.

[154] L. Bergstrom, "Dark Matter Evidence, Particle Physics Candidates and Detection Methods", *Annalen Phys.* **2012**, *524*, 479–496.

[155] T. Blum, P. A. Boyle, V. Gülpers, T. Izubuchi, L. Jin, C. Jung, A. Jüttner, C. Lehner, A. Portelli, J. T. Tsang, "Calculation of the hadronic vacuum polarization contribution to the muon anomalous magnetic moment", *Phys. Rev. Lett.* **2018**, *121*, 022003.

[156] B. Bhattacharya, D. London, J. M. Cline, A. Datta, G. Dupuis, "Quark-flavored scalar dark matter", *Phys. Rev. D* **2015**, *92*, 115012.

[157] J. Kawamura, S. Okawa, Y. Omura, "Interplay between the $b \to sll$ anomalies and dark matter physics", *Phys. Rev. D* **2017**, *96*, 075041.

[158] J. M. Cline, J. M. Cornell, "R(K(∗)) from dark matter exchange", *Physics Letters B* **2018**, *782*, 232–237.

[159] Cerdeño, D. G., Cheek, A., Martín-Ramiro, P., Moreno, J. M., "B anomalies and dark matter: a complex connection", *Eur. Phys. J. C* **2019**, *79*, 517.

[160] B. Barman, D. Borah, L. Mukherjee, S. Nandi, "Correlating the anomalous results in $b \to s$ decays with inert Higgs doublet dark matter and the muon $g-2$", *Phys. Rev. D* **2019**, *100*, 115010.

[161] T. Blum, P. A. Boyle, V. Gülpers, T. Izubuchi, L. Jin, C. Jung, A. Jüttner, C. Lehner, A. Portelli, J. T. Tsang, "Calculation of the Hadronic Vacuum Polarization Contribution to the Muon Anomalous Magnetic Moment", *Phys. Rev. Lett.* **2018**, *121*, 022003.

[162] A. Datta, J. Kumar, D. London, "The B anomalies and new physics in b→se+e", *Physics Letters B* **2019**, *797*, 134858.

[163] A. Crivellin, L. Schnell, "Complete Lagrangian and set of Feynman rules for scalar leptoquarks", *Computer Physics Communications* **2022**, *271*, 108188.

[164] M. Algueró, B. Capdevila, S. Descotes-Genon, J. Matias, M. Novoa-Brunet, $b \to s\ell\ell$ Global Fits after R_{K_S} and $R_{K^{*+}}$, **2021**.

[165] T. Gershon, "Overview of the Cabibbo–Kobayashi–Maskawa matrix", *Pramana* **2012**, *79*, 1091–1108.